

**The Thermal Stability of Anodic Oxide Coatings – Strength and Durability of
Adhesively Bonded Ti-6Al-4V Alloy**

by

Rajesh Kumar Tiwari

Dissertation submitted to the Faculty of the
Virginia Polytechnic Institute and State University
in partial fulfillment of the requirements for the degree of
Doctor of Philosophy
in
Chemistry

Approved:

J. G. Dillard, Chairman

H. C. Dorn

T. C. Ward

J. O. Glanville

M. R. Anderson

Keywords : titanium 6Al-4V ; FM-5 adhesive ; polyimide ; chromic acid anodization ; oxide stability ; thermal treatment ; durability ; aluminum fluoride ; wedge test ; lap shear test

July 18, 2002
Blacksburg, Virginia

The Thermal Stability of Anodic Oxide Coatings – Strength and Durability of Adhesively Bonded Ti-6Al-4V Alloy

by

Rajesh Kumar Tiwari

Chairman: Prof. J.G. Dillard

Center for Adhesive and Sealant Science
Department of Chemistry
Virginia Polytechnic Institute and State University
Blacksburg, Virginia 24061

ABSTRACT

The lap shear strength of chromic acid anodized, primed, Ti-6Al-4V alloy bonded with a high performance FM-5 polyimide adhesive has been investigated as a function of thermal treatment for selected times at various temperatures in air. The research findings indicate that the lap shear strength decreases with the increase in duration of the thermal treatment at constant temperature and with the increase in temperature at constant time. The bond fails increasingly in the oxide coating with increasing treatment temperature and time of treatment. Surface analysis results for debonded specimens suggest that the process leading to failure is the formation of fluorine-containing materials (AlF_3 , $\text{Al}(\text{OF})_n^{3-3n}$, AlF_n^{3-n}) within the oxide, which weakens the adherend-adhesive bond. The formation of the fluorine components is facilitated by treatment at elevated temperatures. This study suggests that the presence of fluoride ions in the anodic oxide coating, prior to bonding, is detrimental to the bond strength of adhesively bonded Ti-alloy when exposed to high temperatures.

The wedge test configuration was used to investigate the influence of temperature on the bond durability of adhesively bonded chromic acid anodized Ti-6Al-4V alloy in air. Based on the average crack length vs. exposure time data, the bond durability varied in the order $-25^\circ\text{C} >$

24°C > 177°C. In each case, the bonded joint failed cohesively within the adhesive, irrespective of the temperature of exposure. XPS analysis and scanning electron photomicrographs of failure surfaces revealed that the failure occurred at the scrim cloth/adhesive interface.

The influence of thermal treatment history on the bond durability of adhesively bonded chromic acid anodized Ti-6Al-4V alloy immersed in boiling water was also investigated. The average crack length vs. immersion time indicated no significant differences for specimens that were thermally treated and then bonded compared to the non-thermally treated specimens. In addition, the failure mode was cohesive within the adhesive for specimens prepared using various thermal treatment conditions. The crack growths for samples treated for 0.5 hour and 1.0 hour and for non-thermally treated specimens for any given exposure time were equivalent. In addition, cohesive failure (failure within adhesive) was observed for each specimen under each treatment condition. The specimens that were bonded and then thermally treated for 3 hours, failed in the oxide coating immediately upon insertion of the wedge. Surface analysis results for debonded specimens suggest that the process leading to failure is the formation of fluorine-containing materials (AlF_3 , $\text{Al}(\text{OF})_n^{3-3n}$, AlF_n^{3-n}) within the oxide. The measured average activation energy for the formation of aluminum fluoride species is 149 kJ/mol. The high activation energy suggests that the rate of aluminum fluoride formation is substantial only at high temperatures.

In summary, the presence of fluorides in the anodic oxide coatings prior to bonding is detrimental to the overall strength and durability of adhesively bonded chromic acid anodized Ti-6Al-4V joints which have been exposed to high temperatures (350°C–399°C).

Dedication

I dedicate this work to my beloved parents, late *Shri Shitala Prasad Tiwari* (Babuji) and *Smt. Narbada Tiwari (Maa)*. My parents have always been a great source of strength, encouragement and love throughout my life. Their constant love and encouragement made it possible for me to reach one of my important educational goals today. I wouldn't have reached this far without their blessings.

Acknowledgments

I would like to express my deep sense of gratitude to my mentor Prof. J. G. Dillard for his advise, support and encouragement during the course of this work. Prof. J. G. Dillard helped me grow professionally and trained me to work independently. I am grateful to him for his patience and understanding during the writing of this dissertation. I thoroughly enjoyed working with him, he is a great Guru.

I want to thank my committee members Prof. T. C. Ward, Prof. H. C. Dorn, Prof. J. O. Glanville and Prof. M. R. Anderson for their helpful technical discussions and encouragement during the course of this work. As an instructor for general chemistry laboratory and physical chemistry laboratory, I received good training in improving my teaching skills under the esteemed guidance of Professors J.O. Glanville and H.C. Dorn, respectively. I specially want to thank Prof. Anderson for his advise, help and support on many issues during my entire stay in Blacksburg. I enjoyed and learned a lot about polymer chemistry and adhesives in particular from Professor T.C. Ward's classes. I also want to thank my former advisor, Prof. G.A. Schick, currently at Eastern Kentucky University, Kentucky, for introducing me to the exciting, challenging and interesting research area of surface chemistry.

I am grateful to National Science Foundation – Science and Technology Center: High Performance Polymeric Adhesive and Composites, NASA-Langley Research Center, Center for Adhesive and Sealant Science, Commonwealth of Virginia – Equipment Trust Fund for the financial support.

I want to thank Boeing Commercial Airplane Company for providing bonded lap shear finger panels and Cytec Company for supplying FM-5 polyimide adhesive.

I want to thank Mr. Frank Cromer, Department of Chemistry, Virginia Tech, for providing technical support in using different analytical tools, such as XPS, AES, SEM/EDAX and SIMS.

Mr. Cromer taught me many finer details about various surface analytical techniques, which are difficult to learn from simply reading books.

I am grateful to Mr. Steve McCartney, Department of Materials Science and Engineering, Virginia Tech, for his help with atomic force microscopy and high resolution scanning electron microscopy work.

I want to thank Dr. Hari Parvatareddy, now at Dow Chemical, Midland, Michigan, from Prof. Dave Dillard's research group in Engineering Science and Mechanics at Virginia Tech, for helping me with testing of lap shear specimens.

I would like to thank Maggie Bump for her help with nano-indentation experiments on FM-5 adhesive and anodic oxide film of Ti-6Al-4V alloy.

I would like to thank past and present students from Prof. J. G. Dillard's research group for their friendship and help during the course of my Ph.D. work. In particular, I would like to thank William Heard, Chris Creegan, Lars Aartun, Brenda Jackson, Sumitra Subrahmanyam, Ron DiFelice, and Owen Hewitt.

I want to thank Department of Chemistry, Virginia Polytechnic Institute and State University, Blacksburg, Virginia for giving me an opportunity to learn and pursue my interest in chemistry at their facility.

I want to thank The Center for Adhesive and Sealant Science (CASS) and the Adhesive and Sealant Council for providing numerous opportunities to attend and present technical papers and posters at various conferences and meetings. I want to thank members of CASS staff for their help during the course of my graduate work. I especially want to thank Ms. Linda Haney, Ms. Kim Mills, Ms. Katy Hatfield, and Ms. Tammy Jo Hiner.

I take this opportunity to thank my parents, late Shri Shitala Prasad Tiwari and Smt. Narbada Tiwari for their love, support and encouragement during the course of my graduate work.

I want to thank my sisters Mrs. Madhu Pandey and Mrs. Sandhya Tripathi and my brothers Dr. Satish K. Tiwari and Dr. Anil K. Tiwari for their love and support. I also want to thank my brother-in-laws, Dr. Ajay K. Pandey and Mr. Neeraj Tripathi, and my sister-in-laws Mrs. Indu Tiwari and Mrs. Sunita Tiwari for their support. Incidentally, three members from my family graduated from Virginia Tech in the past 15 years. This shows our family's love and appreciation for this great institution of higher learning.

Finally, I want to thank my wife, Seema, for her love and understanding during the course of my dissertation writing. If it were not for her understanding and support, it would have taken me even much longer (!) to write my dissertation while working on a full time job and looking after our lovely daughter, Ankita (Jhilmil).

Table of Contents

ABSTRACT	II
DEDICATION	IV
ACKNOWLEDGMENTS	V
CHAPTER 1	1
1.1 THESIS STATEMENT	1
1.2 INTRODUCTION	1
1.3 RESEARCH OBJECTIVES	4
1.4 OVERVIEW	4
CHAPTER 2. LITERATURE REVIEW	6
2.1 ADHESION THEORY	6
2.1.1 <i>Mechanical interlocking theory</i>	6
2.1.2 <i>Adsorption Theory</i>	7
2.1.3 <i>Diffusion Theory</i>	8
2.1.4 <i>Electrostatic Theory</i>	8
2.2 SURFACE PRETREATMENT	9
2.2.1 <i>Mechanical Cleaning</i>	10
2.2.2 <i>TURCO 5578 Etch</i>	10
2.2.3 <i>Acid Etchants</i>	11
2.2.4 <i>Phosphate-Fluoride (P/F) Treatment</i>	11
2.2.5 <i>Pasa-Jell Treatment</i>	12
2.2.6 <i>Vought Abrasive Surface Treatment (VAST)</i>	13
2.2.7 <i>Chromic Acid Anodizing</i>	13
2.2.8 <i>Plasma Treatment</i>	13
2.3 TITANIUM ALLOY (Ti-6Al-4V)	16

2.4 ANODIC OXIDE COATINGS OF Ti-6AL-4V ALLOY AND THEIR HYGRO-THERMAL STABILITY....	16
2.5 DURABILITY OF ADHESIVELY BONDED TITANIUM.....	20
2.6 FLUORIDE IONS IN OXIDE COATINGS: THERMODYNAMIC CONSIDERATIONS OF THEIR REACTIVITY WITH THE ALLOYING METALS AND THEIR OXIDES	24
2.7 THERMAL STABILITY OF POLYIMIDE ADHESIVES.....	29
2.8 BONDING CONFIGURATIONS	30
2.8.1 <i>Single Lap Shear Test Geometry</i>	31
2.8.2 <i>Wedge Test Geometry</i>	31
2.9 ANALYTICAL TECHNIQUES FOR MATERIAL AND SURFACE CHARACTERIZATION	36
2.9.1 <i>Fourier Transform Infrared Spectroscopy</i>	36
2.9.2 <i>X-ray Photoelectron Spectroscopy (XPS)</i>	37
2.9.3 <i>Auger Electron Spectroscopy (AES)</i>	39
2.9.4 <i>Scanning Electron Microscopy (SEM)</i>	41
2.9.5 <i>Secondary Ion Mass Spectrometry (SIMS)</i>	42
2.10 MOTIVATION FOR THE PRESENT RESEARCH WORK	43
CHAPTER 3. EXPERIMENTAL METHODS.....	45
3.1 MATERIALS.....	45
3.2 SURFACE PREPARATION.....	48
3.2.1 <i>Chromic Acid Anodization (CAA)</i>	48
3.2.2 <i>Priming</i>	49
3.3 BOND FABRICATION.....	50
3.4 THERMAL TREATMENT	50
3.5 MATERIAL CHARACTERIZATION.....	52
3.5.1 <i>FM-5 adhesive characterization</i>	52
3.5.2 <i>Adherend characterization</i>	52
3.6 TEST METHODS.....	53
3.6.1 <i>Wedge Test</i>	53
3.6.2 <i>Lap Shear Test</i>	54

3.7 ANALYTICAL TECHNIQUES	55
3.7.1 <i>Fourier Transform Infrared Spectroscopy</i>	55
3.7.2 <i>X-ray Photoelectron Spectroscopy (XPS)</i>	56
3.7.3 <i>Auger Electron Spectroscopy (AES)</i>	57
3.7.4 <i>Secondary Ion Mass Spectrometry (SIMS)</i>	57
3.7.5 <i>Scanning Electron Microscopy (SEM)</i>	58
3.7.6 <i>Atomic Force Microscopy (AFM)</i>	58
3.7.7 <i>Differential Scanning Calorimetry (DSC)</i>	59
3.7.8 <i>Thermogravimetric Analysis (TGA)</i>	59
CHAPTER 4. RESULTS AND DISCUSSION.....	61
4.1 FM-5 ADHESIVE CHARACTERIZATION.....	61
4.1.1 <i>XPS Characterization of FM-5 Adhesive</i>	61
4.1.2 <i>DSC and TGA characterization of FM-5 Adhesive</i>	72
4.1.3 <i>FTIR Characterization of FM-5 Adhesive</i>	75
4.2 SEM, AFM, AES AND XPS CHARACTERIZATION OF THE CAA OXIDE ON Ti-6Al-4V ALLOY	
.....	78
4.2.1 <i>Field Emission Scanning Electron Microscopy (FE-SEM) Characterization</i>	81
4.2.2 <i>Atomic Force Microscopy Characterization</i>	84
4.2.3 <i>SIMS Characterization of the CAA Oxide on Ti-6Al-4V Alloy</i>	93
4.2.4 <i>AES Characterization</i>	99
4.2.5 <i>XPS Characterization</i>	108
4.3 WEDGE TEST RESULTS	126
4.3.1 <i>Influence of temperature on the durability of CAA Ti-6Al-4V/FM-5 bonded joints</i>	126
4.3.1.1 <i>Wedge Test Data</i>	126
4.3.1.2 <i>XPS Surface Analysis of Failure Surfaces</i>	130
4.3.1.3 <i>FTIR Characterization of Failure Surfaces</i>	141
4.3.1.4 <i>Surface Characterization of Failure Surfaces by SEM</i>	142

4.3.2 Influence of Thermal History on the Durability of CAA Ti-6Al-4V/FM-5 Bonded Joints	142
4.3.2.1 Wedge Test Data.....	142
4.3.2.2 Surface Characterization of Failure Surfaces by SEM.....	153
4.3.2.3 Surface Characterization of Failure Surfaces by Diffuse Reflectance FTIR	161
4.3.2.4 XPS Surface Analysis of Failure Surfaces	161
4.4 LAP SHEAR TEST RESULTS.....	179
4.4.1 Non-thermally Treated Specimens.....	179
4.4.2 Thermally Treated Lap Specimens	182
4.4.2.1 Lap Specimens Thermally Treated at 177°C and 204°C (Bond and Heat).....	182
4.4.2.2 Lap Specimens Thermally Treated at Elevated Temperatures (350°C-399°C) ...	187
4.4.2.3 Kinetics of Lap-joint Failure	225
CHAPTER 5. CONCLUSIONS AND SUMMARY.....	233
REFERENCES.....	237
VITA.....	248

List of Figures

Figure 2.1.	The four most common stress-types: (a) shear, (b) normal, (c) cleavage and (d) peel.....	32
Figure 2.2.	A schematic diagram of elastic stress distribution (non-uniform) in the adhesive layer.....	33
Figure 2.3.	A schematic diagram of a typical wedge specimen.....	35
Figure 3.1.	The molecular structure of LaRC PETI-5 adhesive resin ($\langle M_n \rangle = 5,000$ g/mol.).....	47
Figure 3.2.	A schematic diagram showing the adhesive bonding time-temperature curing profile for FM-5/Ti-6Al-4V bonded joints.	51
Figure 4.1.	The carbon (C 1s) and oxygen (O 1s) XPS photopeaks for cured FM-5 adhesive in the bulk region.....	63
Figure 4.2.	The nitrogen (N 1s) and silicon (Si 2p) XPS photopeaks for cured FM-5 adhesive in the bulk region.....	64
Figure 4.3.	The carbon (C 1s) and oxygen (O 1s) XPS photopeaks for cured FM-5 adhesive in the surface region.....	65
Figure 4.4.	The nitrogen (N 1s) and silicon (Si 2p) XPS photopeaks for cured FM-5 adhesive in the surface region.....	66
Figure 4.5	The DSC trace of cured FM-5 adhesive.....	73
Figure 4.6.	The TGA trace of FM-5 adhesive in air. A dotted line is drawn to show the temperature corresponding to a 5% weight loss.....	76
Figure 4.7.	The diffuse reflectance FTIR spectrum (normalized) of cured FM-5 adhesive; (a) without dispersion correction and (b) after dispersion correction.	77
Figure 4.8.	The diffuse reflectance FTIR spectrum (normalized) of uncured neat LaRC PETI-5 powder.....	79
Figure 4.9.	The FE-SEM photomicrographs of oxide coating of CAA Ti-6Al-4V alloy; (a) at 25k magnification and (b) at 200k magnification.	82

Figure 4.10.	The FE-SEM photomicrographs of oxide coating of CAA Ti-6Al-4V alloy which was thermally treated in air at 371°C for 3 hours; (a) at 25k magnification and (b) at 200k magnification.....	83
Figure 4.11.	The FE-SEM photomicrographs of oxide coating of CAA Ti-6Al-4V alloy which was exposed to boiling water for 0.5 hour; (a) at 25k magnification and (b) at 250k magnification.....	85
Figure 4.12.	The AFM image of oxide surface of CAA Ti-6Al-4V alloy; (a) a two-dimensional view and (b) a three-dimensional view.	86
Figure 4.13	The AFM image of oxide surface of CAA Ti-6Al-4V alloy which was thermally treated at 371°C for 3 hours in air; (a) a two-dimensional view and (b) a three-dimensional view.....	87
Figure 4.14.	The AFM image of oxide surface of CAA Ti-6Al-4V alloy which was exposed to de-ionized boiling water for 0.5 hour; (a) a two-dimensional view and (b) a three-dimensional view.....	89
Figure 4.15.	The AFM image of oxide surface of CAA Ti-6Al-4V alloy which was exposed to de-ionized boiling water for 15 hours; (a) a two-dimensional view and (b) a three-dimensional view.....	90
Figure 4.16	The AFM image of oxide surface of CAA Ti-6Al-4V alloy which was exposed to de-ionized boiling water for 192 hours; (a) a two-dimensional view and (b) a three-dimensional view.	91
Figure 4.17.	Positive-ion SIMS spectrum of the oxide surface (top 5 nm) for CAA Ti-6Al-4V alloy.....	94
Figure 4.18.	Negative-ion SIMS spectrum of the oxide surface (top 5 nm) for CAA Ti-6Al-4V alloy.....	95
Figure 4.19.	Negative-ion SIMS spectrum of bulk oxide (at a depth of 30-35 nm from the surface) for CAA Ti-6Al-4V alloy.	100
Figure 4.20.	AES dN(E)/dE derivative (N=5) spectrum for CAA Ti-6Al-4V.	102
Figure 4.21.	AES sputter-depth profile for CAA Ti-6Al-4V alloy.....	103

Figure 4.22.	AES $dN(E)/dE$ derivative ($N=5$) spectrum for a CAA Ti-6Al-4V alloy that was thermally treated at 371°C for 0.5 hour in air.....	105
Figure 4.23.	AES sputter-depth profile for a CAA Ti-6Al-4V alloy specimen that was thermally treated at 371°C for 0.5 hour in air.....	106
Figure 4.24.	AES sputter-depth profile for a CAA Ti-6Al-4V alloy specimen that was thermally treated at 371°C for 24 hours in air.....	107
Figure 4.25.	XPS sputter-depth profile results for the C 1s photopeak as a function of oxide depth for CAA Ti-6Al-4V.....	110
Figure 4.26.	XPS sputter-depth profile results for the O 1s photopeak as a function of oxide depth for CAA Ti-6Al-4V.....	112
Figure 4.27.	XPS sputter-depth profile results for the Al 2p photopeak as a function of oxide depth for CAA Ti-6Al-4V.....	114
Figure 4.28.	XPS sputter-depth profile results for the Ti 2p photopeak as a function of oxide depth for CAA Ti-6Al-4V.....	115
Figure 4.29.	XPS sputter-depth profile results for the F 1s photopeak as a function of oxide depth for CAA Ti-6Al-4V.....	118
Figure 4.30.	High resolution oxygen (O 1s) XPS photopeaks for a CAA Ti-6Al-4V specimen that was (a) immersed in boiling water for 0.5 hr and (b) immersed in boiling water for 192 hrs.....	123
Figure 4.31.	High resolution oxygen (O 1s) XPS photopeaks for a CAA Ti-6Al-4V specimen that was (c) non-treated and (d) thermally treated at 371°C for 3 hrs in air.....	124
Figure 4.32.	Wedge test crack length data for CAA Ti-6Al-4V bonded with FM-5 adhesive and exposed to various temperatures. The crack length results are average data for five specimens per testing temperature.....	127
Figure 4.33.	The strain energy release data for CAA Ti-6Al-4V bonded with FM-5 adhesive and exposed to various temperatures. The strain energy release rate results are average data for five specimens per testing temperature.....	129

Figure 4.34.	The carbon (C 1s) and oxygen (O 1s) XPS photopeaks for side B failure surface of a representative wedge specimen that was aged at -25°C in a freezer for 11,400 hours.....	132
Figure 4.35.	The nitrogen (N 1s) and silicon (Si 2p) XPS photopeaks for side B failure surface of a representative wedge specimen that was aged at -25°C in a freezer for 11,400 hours.....	133
Figure 4.36.	The carbon (C 1s) and oxygen (O 1s) XPS photopeaks for side B failure surface of a representative wedge specimen that was aged at 24°C in a desiccator for 11,400 hours.....	134
Figure 4.37.	The nitrogen (N 1s) and silicon (Si 2p) XPS photopeaks for side B failure surface of a representative wedge specimen that was aged at 24°C in a desiccator for 11,400 hours.....	135
Figure 4.38.	The carbon (C 1s) and oxygen (O 1s) XPS photopeaks for side B failure surface of a representative wedge specimen that was aged at 177°C in a forced-air oven for 11,400 hours.....	136
Figure 4.39.	The nitrogen (N 1s) and silicon (Si 2p) XPS photopeaks for side B failure surface of a representative wedge specimen that was aged at 177°C in a forced-air oven for 11,400 hours.....	137
Figure 4.40.	The diffuse reflectance FTIR spectrum of side B failure surface of a wedge specimen that was aged at 177°C for 11,400 hrs; (a) without dispersion correction and (b) after dispersion correction.....	143
Figure 4.41.	SEM photomicrographs of failure surfaces of a representative wedge specimen that was tested at -25°C in a freezer for 11,400 hrs. The two failure surfaces were arbitrarily labeled as side A and side B. The SEM photomicrographs of the two failure surfaces are not necessarily for corresponding spots.....	144
Figure 4.42.	SEM photomicrographs of failure surfaces of a representative wedge specimen that was tested at room temperature (24°C) in a desiccator for 11,400 hrs. The two failure surfaces were arbitrarily labeled as side A and side B. The SEM	

	photomicrographs of the two failure surfaces are not necessarily for corresponding spots.	145
Figure 4.43.	SEM photomicrographs of failure surfaces of a representative wedge specimen that was tested at 177°C in a forced-air oven for 11,400 hrs. The two failure surfaces were arbitrarily labeled as side A and side B. The SEM photomicrographs of the two failure surfaces are not necessarily for corresponding spots.	146
Figure 4.44.	Wedge test crack length vs. immersion time in boiling water for CAA Ti-6Al-4V bonded with FM-5 adhesive for non-thermally treated (◊) and for CAA Ti-6Al-4V alloy thermally treated at 371°C for 0.5 hr (), 1.0 hr (Δ) and 3.0 hrs (×) in air and then bonded.....	147
Figure 4.45.	Wedge test crack length vs. immersion time in boiling water for CAA Ti-6Al-4V bonded with FM-5 adhesive for non-thermally treated (◊) and for CAA Ti-6Al-4V alloy bonded and then thermally treated at 371°C for 0.5 hr (), 1.0 hr (Δ) and 3.0 hrs (×) in air.....	149
Figure 4.46.	Strain energy release rate vs. immersion time in boiling water for CAA Ti-6Al-4V bonded with FM-5 adhesive for non-thermally treated (◊) and for CAA Ti-6Al-4V alloy thermally treated at 371°C for 0.5 hr (), 1.0 hr (Δ) and 3.0 hrs (×) in air and then bonded.....	150
Figure 4.47.	Strain energy release rate vs. immersion time in boiling water for CAA Ti-6Al-4V bonded with FM-5 adhesive for non-thermally treated (◊) and for CAA Ti-6Al-4V alloy bonded and then thermally treated at 371°C for 0.5 hr () and 1.0 hr (Δ) in air.	151
Figure 4.48.	SEM photomicrographs of failure surfaces of a representative as-bonded specimen (no heat treatment) that was immersed in boiling water for 144 hrs. The SEM photomicrographs of the two failure surfaces are not necessarily for corresponding spots.	154

Figure 4.49.	SEM photomicrographs of failure surfaces of a representative wedge specimen that was thermally-treated at 371°C for 0.5 hours in air and then bonded (heat/bond) and immersed in boiling water for 144 hrs. The SEM photomicrographs of the two failure surfaces are not necessarily for corresponding spots.	155
Figure 4.50.	SEM photomicrographs of failure surfaces of a representative wedge specimen that was thermally-treated at 371°C for 1.0 hour in air and then bonded (heat/bond) and immersed in boiling water for 144 hrs. The SEM photomicrographs of the two failure surfaces are not necessarily for corresponding spots.	156
Figure 4.51.	SEM photomicrographs of failure surfaces of a representative wedge specimen that was thermally-treated at 371°C for 3.0 hours in air and then bonded (heat/bond) and immersed in boiling water for 144 hrs. The SEM photomicrographs of the two failure surfaces are not necessarily for corresponding spots.	157
Figure 4.52.	SEM photomicrographs of failure surfaces of a representative wedge specimen that was bonded and then thermally treated at 371°C for 0.5 hour in air (bond/heat) and immersed in boiling water for 144 hrs. The SEM photomicrographs of the two failure surfaces are not necessarily for corresponding spots.	158
Figure 4.53.	SEM photomicrographs of failure surfaces of a representative wedge specimen that was bonded and then thermally treated at 371°C for 1.0 hour in air (bond/heat) and immersed in boiling water for 144 hrs. The SEM photomicrographs of the two failure surfaces are not necessarily for corresponding spots.	159
Figure 4.54.	SEM photomicrographs of failure surfaces of a representative wedge specimen that was bonded and then thermally treated at 371°C for 3.0 hours in air (bond/heat) and immersed in boiling water for 144 hrs. The SEM	

	photomicrographs of the two failure surfaces are not necessarily for corresponding spots.	160
Figure 4.55.	The diffuse reflectance FTIR spectra of side A and side B failure surfaces for heat/bond wedge specimens that were thermally treated at 371°C for (a) 0.5 hr and (b) 3.0 hrs and then immersed in boiling water for 144 hrs.....	162
Figure 4.56.	The diffuse reflectance FTIR spectra of side A and side B failure surfaces for (a) non-treated wedge specimen and for bond/heat wedge specimens that were thermally treated at 371°C for (b) 0.5 hr and (c) 1.0 hr and then immersed in boiling water for 144 hrs.	163
Figure 4.57.	The diffuse reflectance FTIR spectra of side A and side B failure surfaces for bond/heat wedge specimen that was thermally treated at 371°C for 3.0 hours in air.	164
Figure 4.58.	The carbon (C 1s) XPS photopeak for Side A failure surface for heat/bond wedge specimen that was thermally treated at 371°C for 1 hour in air and then immersed in boiling water for 144 hrs.	169
Figure 4.59.	The carbon (C 1s) XPS photopeak for Side A failure surface for bond/heat wedge specimen that was thermally treated at 371°C for 1 hour in air and then immersed in boiling water for 144 hrs.	171
Figure 4.60.	Auger sputter-depth profiles for the failure surfaces of bond/heat (371°C/3.0 hrs/air)-wedge specimen: (a) Side A and (b) Side B.	173
Figure 4.61.	The curve fit XPS spectra in the aluminum 2p region for (a) the “A” side surface of the failed bond/heat sample (371°C for 3 hours), and for (b) an as-anodized titanium alloy surface.....	174
Figure 4.62.	The curve fit XPS spectra in the fluorine 1s regions for (a) the “A” side surface of the failed bond/heat sample (371°C for 3 hours), and for (b) an as-anodized titanium alloy surface.....	175
Figure 4.63.	SEM photomicrographs of failure surfaces for a non-treated lap specimen.....	180
Figure 4.64.	SEM photomicrographs of failure surfaces for lap specimens thermally treated at 177°C in air for (a) 4 weeks and (b) 4 months.....	184

Figure 4.65.	SEM photomicrographs of failure surfaces for lap specimens thermally treated at 204°C in air for (a) 1 week and (b) 4 weeks.	185
Figure 4.66.	The carbon (C 1s) XPS photopeak for Side A failure surface for a lap specimen thermally treated at 204°C for 4 weeks.	188
Figure 4.67.	The photographs of Side A and Side B failure surfaces for (a) non-treated lap specimen and for specimens that were thermally treated at 399°C for (b) 0.5 hour and 3.0 hours.	190
Figure 4.68.	The SEM photomicrographs of the cohesive failure regions on each failure surface for lap specimens that were thermally treated at 350°C in air for various times; (a) 0.5 hr, (b) 1.0 hr, and (c) 2.0 hrs.	192
Figure 4.68.	(Continued) The SEM photomicrographs of the cohesive failure regions on each failure surface for lap specimens that were thermally treated at 350°C in air for various times; (d) 3.0 hrs, (e) 5.0 hrs, and (f) 11.0 hrs.	193
Figure 4.69.	The SEM photomicrographs of the oxide failure regions on each failure surface for lap specimens that were thermally treated at 350°C in air for various times; (a) 1.0 hr, (b) 2.0 hrs, and (c) 3.0 hrs.	194
Figure 4.69.	(Continued) The SEM photomicrographs of the oxide failure regions on each failure surface for lap specimens that were thermally treated at 350°C in air for various times; (d) 5.0 hrs, (e) 11.0 hrs, and (f) 24 hrs.	195
Figure 4.70.	The SEM photomicrographs of the interfacial failure region for side A and Side B failure surfaces for a lap specimen that was thermally treated at 371°C for 1.0 hr in air.	196
Figure 4.71.	SEM photomicrograph and EDX analysis of interfacial failure region for Side A failure surface for a lap specimen thermally treated at 350°C for 5.0 hrs in air; (a) SEM photomicrograph and (b) EDX analysis results for titanium (Ti), oxygen (O), silicon (Si) and carbon (C).	198
Figure 4.72.	The SEM photomicrographs of the oxide failure regions on each failure surface for lap specimens that were thermally treated at 371°C in air for various times; (a) 0.5 hr and (b) 1.0 hr.	199

Figure 4.72.	(Continued) The SEM photomicrographs of the oxide failure regions on each failure surface for lap specimens that were thermally treated at 371°C in air for various times; (c) 2.0 hrs and (d) 3.0 hrs.....	200
Figure 4.73.	The SEM photomicrographs of the oxide failure regions on each failure surface for lap specimens that were thermally treated at 385°C in air for various times; (a) 0.5 hr and (b) 1.0 hr.	201
Figure 4.73.	(Continued) The SEM photomicrographs of the oxide failure regions on each failure surface for lap specimens that were thermally treated at 385°C in air for various times; (c) 2.0 hrs and (d) 3.0 hrs.....	202
Figure 4.74.	The SEM photomicrographs of the oxide failure regions on each failure surface for lap specimens that were thermally treated at 399°C in air for various times; (a) 0.5 hr and (b) 1.0 hr.	203
Figure 4.74.	(Continued) The SEM photomicrographs of the oxide failure regions on each failure surface for lap specimens that were thermally treated at 399°C in air for various times; (c) 2.0 hrs and (d) 3.0 hrs.....	204
Figure 4.75.	Carbon (C 1s) and oxygen (O 1s) XPS photopeaks for Side A and Side B failure surfaces, in cohesive failure region, for a lap specimen thermally treated at 371°C for 3.0 hours in air.....	216
Figure 4.76.	Nitrogen (N 1s) and silicon (Si 2p) XPS photopeaks for Side A and Side B failure surfaces, in cohesive failure region, for a lap specimen thermally treated at 371°C for 3.0 hours in air.....	217
Figure 4.77.	Carbon (C 1s) and oxygen (O 1s) XPS photopeaks for Side A and Side B failure surfaces, in interfacial failure region, for a lap specimen thermally treated at 371°C for 3.0 hours in air.....	218
Figure 4.78.	Nitrogen (N 1s) and silicon (Si 2p) XPS photopeaks for Side A and Side B failure surfaces, in interfacial failure region, for a lap specimen thermally treated at 371°C for 3.0 hours in air.....	219

Figure 4.79.	Titanium (Ti 2p) and aluminum (Al 2p) XPS photopeaks for Side A and Side B failure surfaces, in interfacial failure region, for a lap specimen thermally treated at 371°C for 3.0 hours in air.....	220
Figure 4.80.	Fluorine (F 1s) XPS photopeaks for Side A and Side B failure surfaces, in interfacial failure region, for a lap specimen bonded and thermally treated at 371°C for 3.0 hrs in air.....	221
Figure 4.81.	Curve-fit XPS analysis of aluminum 2p photopeak in an interfacial failure region for a lap specimen bonded and thermally treated at 371°C for 3.0 hrs in air; (a) Side A failure surface (b) Side B failure surface.....	223
Figure 4.82.	Curve-fit XPS analysis of fluorine 1s photopeak in an interfacial failure region for a lap specimen bonded and thermally treated at 371°C for 3.0 hrs in air; (a) Side A failure surface (b) Side B failure surface.	224
Figure 4.83.	Auger sputter-depth profiles of Side A and Side B failure surfaces for a lap specimen thermally treated at 399°C for 3.0 hrs in air.	226
Figure 4.84.	Concentration of fluorine, as fluoride, plotted vs. the thermal treatment time at various treatment temperatures: (o) 350°C, () 371°C, (Δ) 385°C and (×) 399°C; straight lines are the least-squares fits from the regression analyses.	228
Figure 4.85.	Concentration of aluminum, as fluoride, plotted vs. the thermal treatment time at various treatment temperatures: (◇) 350°C, () 371°C, (Δ) 385°C and (×) 399°C; straight lines are the least-squares fits from the regression analyses.	229
Figure 4.86.	Arrhenius plot: rate of aluminum fluoride formation vs. 1/T : (o) linear rate constants from fluorine kinetic data; (×) linear rate constants from aluminum kinetic data; straight lines are the least-squares fits from the regression analyses.	231

List of Tables

Table 2.1.	Equilibrium chemical equations and calculated standard Gibbs free energy of reaction (Δ_rG°) values at room temperature (298.15°K) and at 700°K.	26
Table 2.2.	The published standard Gibbs free energy of formation (Δ_fG°) values for titanium oxide, aluminum oxide, titanium fluorides, aluminum fluoride, water and hydrofluoric acid at room temperature (298.15°K) and at 700°K.	27
Table 3.1.	The elemental composition of as received titanium alloy, from President Titanium Company, as reported in the material safety data sheet.	46
Table 3.2.	The chemical composition (weight %) of as received FM-5 adhesive film from CYTEC, as reported in the material safety data sheet.	46
Table 4.1.	The elemental compositions (atomic %) of uncured and cured FM-5 adhesive for the surface and bulk regions as determined by XPS analysis.	62
Table 4.2.	The XPS curve-fit analysis results for cured FM-5 adhesive in the bulk region.	67
Table 4.3.	The XPS curve-fit analysis results for cured FM-5 adhesive in the surface region. .	68
Table 4.4.	The XPS curve-fit analysis results for silane treated glass cloth.	71
Table 4.5.	The glass transition temperatures (T_g) for cured FM-5 adhesive as a function of additional heating at 371°C and 399°C, in air.	74
Table 4.6.	The characteristic diffuse reflectance FTIR absorption bands for cured FM-5 adhesive and uncured neat PETI-5 resin.	80
Table 4.7.	Surface-roughness analysis results (from AFM image) for oxide surfaces for CAA Ti-6Al-4V alloy after various treatments.	92
Table 4.8.	SIMS Positive-ion peak assignments for the oxide on CAA Ti-6Al-4V alloy.	96
Table 4.9.	The calculated abundance (wt. %) of titanium isotopes from the positive-ion dynamic SIMS spectrum for CAA Ti-6Al-4V alloy.	98
Table 4.10.	The oxide coating thicknesses for CAA Ti-6Al-4V alloy, as determined from AES sputter-depth profile, as a function of various treatments. The standard deviations are given at the 95% confidence limit.	101

Table 4.11. XPS sputter-depth profile elemental composition data (atomic %) for a CAA oxide on CAA Ti-6Al-4V alloy. The standard deviations are reported at the 95% confidence limit.....	109
Table 4.12. XPS sputter-depth profile/binding energy (eV) data for a CAA oxide on Ti-6Al-4V alloy. The standard deviations are reported at the 95% confidence limit.....	109
Table 4.13. The reference binding energy (B.E.) values for titanium in various oxidation states in titanium oxides as tabulated by McCafferty et al. [197]; titanium B.E. values are with reference to the carbon 1s XPS photopeak at 285.0 eV.	117
Table 4.14. XPS sputter-depth profile data (atomic %) for CAA Ti-6Al-4V thermally treated at 371°C for 3 hrs in air.....	120
Table 4.15. XPS sputter-depth profile data (binding energies) for CAA Ti-6Al-4V alloy, thermally treated at 371°C for 3 hrs in air.	120
Table 4.16. XPS sputter-depth profile data (atomic percent and binding energies) for CAA Ti-6Al-4V immersed in boiling water for 0.5 hr.	122
Table 4.17. XPS sputter-depth profile data (atomic percent and binding energies) for CAA Ti-6Al-4V immersed in boiling water for 192 hrs.....	122
Table 4.18. The XPS O 1s curve-fit analysis results for non-treated, thermally treated and boiling water immersed CAA Ti-6Al-4V alloy.	125
Table 4.19. The surface atomic concentrations of elements, as determined by XPS analysis of failure surfaces of CAA pretreated wedge specimens, exposed to one of the three environments; low temperature (–25°C) in a freezer, room temperature (24°C) in a desiccator and elevated temperature (177°C) in a forced-air oven. Standard deviations are given at the 95% confidence limit.	131
Table 4.20. The XPS curve-fit analysis results for side B failure surface for a wedge specimen aged at –25°C in a freezer for 11,400 hrs.	138
Table 4.21. The XPS curve-fit analysis results for side B failure surface for a wedge specimen aged at 24°C in a desiccator for 11,400 hrs.	139
Table 4.22. The XPS curve-fit analysis results for side B failure surface for a wedge specimen aged at 177°C in a forced-air oven for 11,400 hrs.....	140

Table 4.23. The surface atomic concentrations of elements, as determined by XPS analysis of failure surfaces of as-bonded chromic acid anodized Ti-6Al-4V specimens (non-treated) immersed in de-ionized water for about 144 hours. Standard deviations are given at the 95% confidence limit.....	166
Table 4.24. The surface atomic concentrations of elements, as determined by XPS analysis of failure surfaces of wedge specimens that were prepared by a thermal treatment at 371°C in air for 0.5, 1.0 and 3.0 hours, bonded (heat/bond specimens) and then immersed in boiling water for about 144 hrs. Standard deviations are given at the 95% confidence limit.	167
Table 4.25. The surface atomic concentrations of elements, as determined by XPS analysis of failure surfaces of wedge specimens that were bonded and then thermally treated (bond/heat specimens) at 371°C in air for 0.5, 1.0 and 3.0 hours and then immersed in boiling water for about 144 hours. Standard deviations are given at 95% confidence limit.....	170
Table 4.26. XPS results (atomic %) for non-treated lap specimens. Two different failure surfaces of the same lap specimen analyzed; arbitrarily labeled side A and side B. Standard deviations are reported at the 95% confidence limit.	181
Table 4.27. The lap-shear strengths and failure modes (visual) for specimens thermally treated in air at 177°C and 204°C for various times. Standard deviations are reported at the 95% confidence limit.	183
Table 4.28. XPS results (atomic %) for lap specimens thermally treated at 177°C, in air, for 4 weeks and 4 months. Standard deviations are reported at the 95% confidence limit.	186
Table 4.29. XPS results (atomic %) for lap specimens thermally treated at 204°C, in air, for 1 week and 4 weeks. Standard deviations are reported at the 95% confidence limit.	186
Table 4.30. The lap-shear strengths and failure modes (visual) for specimens thermally treated in air at 350°C, 371°C, 385°C and 399°C for various times. Standard deviations are reported at the 95% confidence limit.....	189

Table 4.31. XPS results (atomic %) for both failure surfaces in the cohesive failure region for lap specimens thermally treated at 350°C for 0.5 hour, in air. Standard deviations are reported at the 95% confidence limit.....	197
Table 4.32. XPS results (atomic %) for both failure surfaces in the cohesive failure region and interfacial failure region for lap specimens thermally treated at 350°C for 1.0 hour, in air. Standard deviations are reported at the 95% confidence limit.	205
Table 4.33. XPS results (atomic %) for both failure surfaces in the cohesive failure region and interfacial failure region for lap specimens thermally treated at 350°C for 2.0 hours, in air. Standard deviations are reported at the 95% confidence limit.	206
Table 4.34. XPS results (atomic %) for both failure surfaces in the cohesive failure region and interfacial failure region for lap specimens thermally treated at 350°C for 3.0 hours, in air. Standard deviations are reported at the 95% confidence limit.	206
Table 4.35. XPS results (atomic %) for both failure surfaces in the cohesive failure region and interfacial failure region for lap specimens thermally treated at 350°C for 5.0 hours, in air. Standard deviations are reported at the 95% confidence limit.	207
Table 4.36. XPS results (atomic %) for both failure surfaces in the cohesive failure region and interfacial failure region for lap specimens thermally treated at 350°C for 11.0 hours, in air. Standard deviations are reported at the 95% confidence limit.	207
Table 4.37. XPS results (atomic %) for both failure surfaces in the interfacial failure region for lap specimens thermally treated at 350°C for 24.0 hours, in air. Standard deviations are reported at the 95% confidence limit.....	208
Table 4.38. XPS results (atomic %) for both failure surfaces in the cohesive failure region and interfacial failure region for lap specimens thermally treated at 371°C for 0.5 hour, in air. Standard deviations are reported at the 95% confidence limit.	209
Table 4.39. XPS results (atomic %) for both failure surfaces in the cohesive failure region and interfacial failure region for lap specimens thermally treated at 371°C for 1.0 hour, in air. Standard deviations are reported at the 95% confidence limit.	209

Table 4.40. XPS results (atomic %) for both failure surfaces in the cohesive failure region and interfacial failure region for lap specimens thermally treated at 371°C for 2.0 hours, in air. Standard deviations are reported at the 95% confidence limit.	210
Table 4.41. XPS results (atomic %) for both failure surfaces in the cohesive failure region and interfacial failure region for lap specimens thermally treated at 371°C for 3.0 hours, in air. Standard deviations are reported at the 95% confidence limit.	210
Table 4.42. XPS results (atomic %) for both failure surfaces in the cohesive failure region and interfacial failure region for lap specimens thermally treated at 385°C for 0.5 hour, in air. Standard deviations are reported at the 95% confidence limit.	211
Table 4.43. XPS results (atomic %) for both failure surfaces in the cohesive failure region and interfacial failure region for lap specimens thermally treated at 385°C for 1.0 hour, in air. Standard deviations are reported at the 95% confidence limit.	211
Table 4.44. XPS results (atomic %) for both failure surfaces in the interfacial failure region for lap specimens thermally treated at 385°C for 2.0 hours, in air. Standard deviations are reported at the 95% confidence limit.	212
Table 4.45. XPS results (atomic %) for both failure surfaces in the interfacial failure region for lap specimens thermally treated at 385°C for 3.0 hours, in air. Standard deviations are reported at the 95% confidence limit.	212
Table 4.46. XPS results (atomic %) for both failure surfaces in the cohesive failure region and interfacial failure region for lap specimens thermally treated at 399°C for 0.5 hour, in air. Standard deviations are reported at the 95% confidence limit.	213
Table 4.47. XPS results (atomic %) for both failure surfaces in the cohesive failure region and interfacial failure region for lap specimens thermally treated at 399°C for 1.0 hour, in air. Standard deviations are reported at the 95% confidence limit.	213
Table 4.48. XPS results (atomic %) for both failure surfaces in the interfacial failure region for lap specimens thermally treated at 399°C for 2.0 hours, in air. Standard deviations are reported at the 95% confidence limit.	214

Table 4.49. XPS results (atomic %) for both failure surfaces in the interfacial failure region for lap specimens thermally treated at 399°C for 3.0 hours, in air. Standard deviations are reported at the 95% confidence limit.....	214
Table 4.50. Linear rate constants for the aluminum – fluorine reaction.....	230

Chapter 1

1.1 Thesis statement

The presence of fluoride in the anodic oxide coatings is detrimental to the overall strength and durability for adhesively bonded chromic acid anodized Ti-6Al-4V joints which have been exposed to high temperatures (350°C – 399°C).

1.2 Introduction

Adhesively bonded joints are preferred over the conventional methods of joining metals such as, riveting, welding, bolting and soldering [1]. Some of the main advantages of adhesively bonded joints compared to conventional joints are the ability to join dissimilar materials (thin metallic and/or non metallic sheets), better stress distribution, higher joint efficiency index (a measure of relative strength to weight ratio of the bonded region) and lower fabrication costs [1]. The excellent thermal and insulation properties, superior damping and noise reduction properties and an improvement in corrosion resistance are also advantages of adhesively bonded joints [2,3]. However, adhesively bonded joints have some limitations compared to conventional joining methods. Compared to metals, the adhesives have a lower toughness and strength in compression and tension and hence are not used for joining thick metallic components unless the bonded area is large. Adhesives also have a relatively low thermal stability and hence adhesively bonded joints have limited high temperature applications. The substrate may also require an elaborate surface preparation prior to bonding. An elaborate substrate preparation is a costly and a time consuming procedure. To make a strong and durable joint the substrates and adhesives are selected after carefully reviewing the joint design and the service environment requirements. Adhesively bonded joints must satisfy the design criteria and also perform satisfactorily in the service environments.

In an adhesively bonded joint a stronger physical and chemical interaction between the substrate surface and the adhesive is desired. A strong and durable joint can be fabricated by suitably modifying the physical and chemical properties of the substrate surface and/or of the adhesive. Since most metals have natural oxide coatings on their surfaces, the adhesive interacts directly with the natural oxide coating and not with the metal. Usually, the natural oxide coatings on metal surfaces do not have the desired physical or chemical properties to form a good adhesively bonded joint. For example, the natural oxide coatings on copper metal do not adhere well to the underlying metal surface [4]. In general, metal surfaces also have unwanted hydrocarbon contamination from the atmosphere which must be removed for a better oxide/adhesive interaction. Therefore, almost always the metal surfaces are physically and/or chemically treated (surface pretreatment) to create and/or alter the properties of the surface to make it compatible with the adhesive.

A wide variety of mechanical and chemical treatments can be used to treat the metal surfaces. Chromic acid anodization (CAA) is an excellent surface pretreatment for preparing metal surfaces, particularly for aluminum and titanium, for adhesive bonding [5,6]. However, a surface prepared via CAA is limited to service environments where the temperature does not exceed 200°C [7]. The anodic oxide coatings grown via CAA on Ti-6Al-4V alloy are thermally unstable at high temperatures (>300°C) [8,9]. However, despite CAA being one of the best surface pretreatments for titanium alloys for adhesive bonding, the lack of a complete understanding of the thermal stability of anodic oxide coatings has not allowed the realization of the full potential of the CAA treatment for adhesive bonding in high temperature applications.

Ti-6Al-4V alloy is an important construction material for high-speed aircraft. The high speed civil transport (HSCT) aircraft is designed to travel up to a maximum speed of Mach 2.4 and to have more than 60,000 hours of service life. The flying conditions are such that the aircraft is expected to encounter high service temperatures, in the vicinity of 177°C to 204°C. For several reasons, and primarily for improved stress distribution and higher strength to weight ratio, it is desirable to fabricate and use adhesively bonded joints for many components in the proposed

aircraft. For this application, a high performance scrim cloth supported polyimide adhesive film, FM-5 (Cytec), is appropriate for adhesive bonding. However, the physical and/or chemical degradation of the adhesive and the oxide coatings at 177°C and 204°C must be investigated in detail to assure performance. Also, since many high performance polyimide adhesives cure in the range of 350° to 400°C, good thermal stability of the oxide coating is desired.

The presence of some specific chemical species, such as, phosphates, magnesium, copper and fluoride ions in the oxide coatings influence the stability of the oxide film in various environments [10-14]. The presence of phosphate ions in oxide coatings inhibits or delays hydration of oxide films of aluminum alloys when exposed to water or moisture, thus preventing the formation of a mechanically weak hydrated oxide coating on the surface [10,11]. The hydrated oxide film adheres poorly to the base alloy and thus becomes a weak link in the adhesively bonded joint. Similarly, compared to the bulk of the alloy, a lower aluminum-to-magnesium ratio in the oxide coating (presence of a relatively higher concentration of magnesium ions in the oxide coatings) of an aluminum alloy results in poor joint durability [10]. The presence of small amounts of chloride (Cl⁻) and/or fluoride (F⁻) ions in the anodization solution or etch solution decreases the height and roughness of the aluminum oxide coating [15]. This decrease in the micro-roughness of the aluminum oxide coating leads to the poor joint performance in a hot-wet environment. Fluoride ions in the aluminum oxide coating could react with ambient moisture to form hydrofluoric acid which further attacks the aluminum oxide structure [16]. However, the influence of such adsorbed and/or absorbed ions on the bond strength and durability has not been fully investigated for titanium alloys. Fluoride is present in a significant amount (3-4 atomic %) as absorbed fluoride ion in the CAA oxide coatings of the titanium alloy [8]. The exact chemical form(s) in which fluoride ions are present in the oxide coating of an anodized alloy has not been studied in detail. Fluoride ions could be present as adsorbed anions [17] and/or in the metal oxide lattice as a substitute (impurity) for O²⁻ ions. Since F⁻ and O²⁻ anions have very similar ionic radii [18], the substitution of fluoride ions (F⁻) for oxide anions (O²⁻) in metal oxides is very common [19,20]. Fluoride ions could also be associated with hydrogen in the form of hydrofluoric acid since metal oxides in general retain

some amount of moisture when exposed to the atmosphere at ambient temperature. Fluoride ions in the anodic oxide coatings could react, if it is thermodynamically feasible, with metals and their oxides to form metal fluorides and/or metaloxyfluorides and other products. Depending on the chemical and physical properties of the new reaction products, their formation could have an important bearing on the strength and durability of a bonded joint. Surprisingly, the influence of fluoride ions on the strength and durability of bonded joints has not been investigated in detail.

1.3 Research Objectives

In this work, the influence of thermal treatment on the strength and durability of Ti-6Al-4V alloy bonded with a high performance scrim cloth-supported polyimide adhesive, FM-5 (Cytec), has been studied. The main objective of this study was to understand the thermal degradation mechanism in the anodic oxide and its influence on the strength and durability of adhesively bonded Ti-6Al-4V alloy joints when exposed to high temperatures. In particular the role of fluorine, which is present as absorbed fluoride ion in the anodic oxide coating, on the durability and strength of bonded joint has been investigated. Finally, a thermal treatment method has been suggested for removing fluorine, which are primarily responsible for the degradation of the anodic oxide coating in the titanium alloy. Overall, the thermal degradation of the anodic oxide coatings and the influence of such degradation on bond strength and durability have been investigated in this work.

1.4 Overview

This dissertation consists of five chapters. The thesis statement is provided in chapter 1 along with a discussion of the advantages and disadvantages of adhesively bonded joints and this is followed by a statement of the research objectives.

Chapter II describes various theories of adhesion, the past and recent work in the area of surface pretreatment for titanium and its alloys, the thermal stability of anodic oxide coatings on Ti-

alloys, the thermal stability of polyimide adhesive, the bond durability of Ti-alloys and bonding configurations.

Experimental methods are presented in chapter III. The test materials, surface preparation, priming, fabrication of test specimens, thermal treatment of specimens, lap shear strength and durability (wedge test) experiments are discussed. Various instrumental techniques used for the characterization of adherend and adhesive film and for the analysis of failure surfaces are also described.

The results and discussion are included in chapter IV. The results of adhesive and substrate material characterization are discussed followed by the wedge test results including the influence of temperature on bond durability in air, and the influence of thermal history on the durability of the adhesively bonded titanium alloy in boiling water. The influence of thermal treatment on the lap shear strength and on the failure modes of adhesively bonded titanium alloy is discussed at the end. The thermal degradation mechanism of the anodic oxide coating and the bond failure mechanism in the adhesively bonded joints are also discussed.

The summary and conclusions of this work are reported in chapter V. Suggested future work arising from the present study is also presented in this chapter.

Chapter 2. Literature Review

2.1 Adhesion Theory

A clear understanding of adhesion mechanisms is of paramount importance if a durable and strong adhesive bond is to be achieved. The various factors affecting bond strength and durability could be optimized for better adhesion if the adhesion mechanism is more fully understood. The adhesion between two surfaces can be improved by removing mechanically weak surface layers, by increasing the substrate surface roughness, surface area and wettability, and by improving the energy dissipative mechanism(s) in the adhesive. Different theories have been proposed to explain adhesion, but the mechanisms are usually system specific. There is no universal adhesion model to explain the adhesion properties of a variety of different bonded joints involving different combinations of substrates and adhesives and exposed to a variety of environments.

Almost all adhesion models can be grouped into one of the following four major adhesion theories that have developed; 1) Mechanical interlocking theory 2) Adsorption theory 3) Diffusion theory and 4) Electronic theory.

2.1.1 Mechanical interlocking theory

The mechanical interlocking theory was proposed by MacBain and Hopkins in 1925 [21]. According to this theory the physical interlocking (mechanical keying) between the adhesive and the adherend surface is primarily responsible for adhesion [22]. Since mechanical keying plays a major role in this mechanism, the adhesive strength is greatly dependent on the topography of the adherend surface. The adherend surface is treated either mechanically and/or chemically to achieve the desired porous and rough adherend surface topography. Chemical treatments involve etching, polishing, anodizing and plasma treatment. Mechanical treatment usually involves scrubbing and polishing with sandpaper and grit blasting. Mechanical interlocking was a

major contributing factor for adhesion of rubber to textile fabrics [23] and for adhesion of molten polyethylene to anodized aluminum surfaces [24]. There are other examples, which clearly show the important role played by mechanical interlocking in the adhesion process [25-27]. However, the theory fails to explain the adhesion between smooth surfaces where mechanical keying is minimal as in the case of adhesion between two atomically smooth mica surfaces [28,29] and between two optically smooth rubber surfaces [29]. In a real world application where most adherend surfaces have a relatively rough topography, mechanical interlocking is believed to play some role in the adhesion process.

2.1.2 Adsorption Theory

According to the adsorption theory, the formation of primary and/or secondary bonds (molecular level forces) between two interacting surfaces is primarily responsible for adhesion. Since chemical interactions are at atomic and molecular levels, an intimate contact between the two interacting surfaces is required. The primary bonds involve ionic, covalent or metallic bonding and the secondary bonds usually involve van der Waals forces and hydrogen bonding between the adhesive and the adherend surface. A third type of molecular force involves a donor-acceptor type interaction (acid-base interaction) between the adhesive and adherend. The bond energies associated with different types of chemical bonds are a good measure of the adhesive strength between the interacting surfaces. The bond energies associated with primary bonds are in the range of 600-1100 kJ/mol for ionic bonds, 60-700 kJ/mol for covalent bonds and 110-350 kJ/mol for metallic bonds [30-32]. Surface analytical tools have provided strong evidence for primary bond formation between adhesive and adherend in some cases [33,34]. In one study, the addition of small reactive functional groups (reactive with adherend) in the adhesive formulation increased the adhesive strength [35].

By comparison, the bond energies associated with secondary bonds are in the range of 10-25 kJ/mol for hydrogen bonds without the involvement of fluorine and up to 40 kJ/mol for hydrogen bonds involving fluorine. The secondary bonds resulting from van der Waals forces of attraction

are in the range of 4-20 kJ/mol for permanent dipole-dipole (van der Waals type) interaction, less than 2 kJ/mol for dipole-induced dipole (van der Waals type) interactions and 0.08-40 kJ/mol for interactions involving dispersion forces. In adhesion studies involving sulfuric acid anodized and chromic acid anodized aluminum surfaces with epoxy adhesives, only secondary forces are involved [36,37]. There are numerous other examples of adhesively bonded joints where interfacial secondary forces between the adhesive and adherend were primarily responsible for adhesion [38-45].

The bond energies associated with a donor-acceptor interactions can be as high as 1000 kJ/mol in some cases involving Bronsted acid-base type interactions, and up to 80 kJ/mol for Lewis acid-base interactions. Donor-acceptor type interactions between the adhesive and adherend can contribute significantly to adhesion forces [30,46,47].

2.1.3 Diffusion Theory

The diffusion theory is used primarily to explain the adhesion between two polymer materials. According to this theory, as explained by Voyutskii [48,49], the inter-diffusion of polymer segments or chains between the two polymers at the interface is responsible for adhesion. Voyutskii [48] demonstrated that the peel adhesive strength for any given pair of polymers is greatly dependent on the relative ease with which the inter-diffusion of molecular chains and/or segments takes place between the polymer pairs. Therefore, for better inter diffusion of polymer segments/chains, the polymers must have closely matched solubility parameters, and also the polymer segments/chains must have sufficient mobility to promote inter diffusion.

2.1.4 Electrostatic Theory

Deryaguin and co-workers [50,51] proposed that the adhesion between two different materials is due to the differences in their electronic band structure. The differences in electronic band structure give rise to the formation of an electrical double layer across the interface, a capacitor,

that results in an electrostatic interaction between the joining surfaces. That the electrostatic forces of attraction play a major role in the adhesion of planar surfaces and particles was clearly demonstrated by Krupp [52,53]. However, in other studies involving adhesion of vacuum deposited metals on glass substrates, the contribution from electrostatic forces due to an electric double layer was negligible compared to the contribution from van der Waals interactions [54]. In another study involving metal/polymer joints, it was found that the electrostatic contribution was very small compared to the van der Waals contribution [55].

2.2 Surface Pretreatment

Since both the initial bond strength and the subsequent bond durability are greatly dependent on the extent of physical and chemical interaction between the adhesive and the adherend surface, the adherend surface topography and the chemical properties of the adherend and the adhesive become very important. Several studies have clearly demonstrated the importance of the surface properties (chemistry) of adherends in adhesion mechanisms [56-59]. The adherend surface is physically and/or chemically treated to enhance the bond strength and durability [5, 60-63]. Weak boundary layers such as weak oxide layers, release agents, and low molecular weight species can be effectively removed from the adherend surface by suitable surface pretreatments [64].

To optimize bonding at the adherend-adhesive interface, the adherend surface is almost always pretreated to some degree prior to adhesive bonding. In general, a surface pretreatment results in an improvement in some or all of the following adherend surface characteristics:

- Increase in surface wettability
- Removal of unwanted weak boundary layers
- Increase in macro- and microroughness
- Increase in chemical and mechanical stability of surface oxides
- Increase in chemical interaction between adhesive and adherend

Surface pretreatments for metal surfaces can be broadly classified into four major groups, namely, mechanical treatment, chemical treatment, electrochemical treatment and plasma treatment. Review articles on surface pretreatments for aluminum [6] and titanium [5] give excellent summaries of the different surface pretreatments that are commonly used. Some of these surface pre-treatments for titanium alloys are discussed below.

2.2.1 Mechanical Cleaning

In this method, the adherend surface is mechanically roughened to remove surface contamination and to increase the macro-roughness of the adherend surface. The removal of surface contaminants helps in preparing the surface for any additional surface pretreatments that may be necessary for any specific applications. Thus, mechanical cleaning is usually the first step involved in any surface pretreatment of an adherend surface. Mechanical cleaning involves scrubbing the substrate surface with wire brushes and/or sandpaper and/or scouring materials like Scotch-Brite™ (3M company). Mechanical cleaning via grit blasting the adherend surface with high speed particles, such as alumina and silica, produces a macro-rough surface morphology. Compared to chemical and electrochemical surface pretreatments, adherends treated via grit-blasting show poor durability [65,7].

2.2.2 TURCO 5578 Etch

TURCO 5578, a proprietary alkaline etchant, was developed at TURCO Products, Inc. USA. An aqueous solution containing TURCO 5578 (6-8 wt.%/vol.) at 80-90°C is usually recommended for surface treatment [66]. The thickness of the amorphous oxide coatings for TURCO treated surfaces is about 18 nm [67], which is thinner than oxide coatings produced via chromic acid anodization (CAA) (45 nm). However, the oxide macroroughness (peak to valley) is 3.4 μm for a TURCO treated surface compared to 2.1 μm for CAA produced oxide coatings [68]. In bond durability studies, adherends surface treated with the TURCO 5578, out-performed phosphate-fluoride (P/F) treated substrates [69, 70]. Adherends treated using CAA or sodium hydroxide

anodization (SHA) exhibited better durability than substrates pretreated using the TURCO 5578 or P/F procedure.

2.2.3 Acid Etchants

Sulfuric acid, nitric-hydrofluoric acid mixtures and hydrochloric-orthophosphoric acid mixtures are some of the common acid pretreatments for titanium alloys [71, 72]. Compared to chromic acid anodization or phosphoric acid anodization, the acid etching, by itself, does not provide superior bondable surfaces. When acid etching is used as a surface pretreatment, the acid dissolves the contaminated natural oxide layers on the adherend surface and replaces the natural oxide with a new bondable oxide coating. Therefore, though acid etching may not be a good surface pretreatment by itself, acid etching forms a very important intermediate step in surface pretreatment processes. One of the major problems associated with acid treatments is hydrogen pick up by the adherend material, which can cause embrittlement of the metal. To minimize hydrogen pick-up a special nitric-hydrofluoric acid mixture having 3% (v/v) hydrofluoric acid (47% HF) and 15% (v/v) nitric acid (Concentrated HNO₃) is used as an etching solution [73].

2.2.4 Phosphate-Fluoride (P/F) Treatment

The phosphate-fluoride treatment involves two steps; first, the adherend surface is etched in a 3% (v/v) hydrofluoric acid (47% HF) and 15% (v/v) nitric acid (concentrated HNO₃) solution followed by immersing the metal in an aqueous solution containing 5% (w/v) anhydrous trisodium phosphate, 2% (w/v) potassium fluoride and 2.6% (v/v) hydrofluoric acid (47% HF) for 2 minutes (US patent 2 864 732). The substrate is finally rinsed with de-ionized water. Chemically, the anatase oxide coating produced via phosphate-fluoride treatment on the titanium alloy consists of titanium, oxygen, phosphorus, fluorine, aluminum and carbon. Carbon is usually present in the form of unavoidable organic contaminants from the atmosphere. The thickness of the oxide coating produced via the phosphate-fluoride etch is in the range of 150 nm to 295 nm

[74]. The oxide macroroughness (peak to valley) is 2.8 μm for a P/F treated surface compared to 2.1 μm for CAA produced oxide coatings [68].

A slightly modified P/F solution, containing 0.75% (w/v) anhydrous sodium sulfate in addition to trisodium phosphate, potassium fluoride and hydrofluoric acid, is used as an effective medium for surface pretreatment [75]. Sodium sulfate is added to prevent degradation of the anatase oxide on the adherend surface when exposed to hot/humid environmental conditions. Compared to the standard phosphate-fluoride treatment, the modified phosphate-fluoride treatment improved the joint durability of Ti-6Al-4V alloy bonded with an epoxy adhesive, when exposed to 95% relative humidity at 50°C [76].

2.2.5 Pasa-Jell Treatment

The exact chemical composition of Pasa-Jell, a propriety formulation of Semco Sales and Services Co., Los Angeles, USA, is not known. Pasa-Jell 107, used for surface pretreatment of titanium, is believed to be composed of approximately 40% nitric acid, 10% fluorides, 10% chromic acid, 1% couplers and water [77]. Pasa-Jell comes either in a solution form where the adherend is immersed in the solution for a specific period of time or in a paste form where the adherend surface is covered with the paste for 10-15 minutes; the immersion or treatment time in Pasa-Jell paste or solution is detrimental to the overall bond durability [71]. Based on durability studies, the liquid form performs slightly better than the paste form of Pasa-Jell [69]. The thickness of the anatase oxide is in the range of 5 nm [7] to 20 nm for adherends treated in liquid Pasa-Jell [78]. The anatase oxide structure formed on the titanium alloy surface is stable up to 175°C but converts to the rutile form when heated to 350°C [79]. In bond durability studies involving titanium adherends in a wedge test configuration and tested in a hot-humid environment (60°C, 100% RH), the liquid Pasa-Jell pretreatment was better than P/F and Vought Abrasive Surface Treatment (VAST) treatments (see below), but inferior to the TURCO 5578 treatment [80-82].

2.2.6 Vought Abrasive Surface Treatment (VAST)

The VAST treatment was developed by the Vought Systems of LTV Aerospace Corporation, Dallas, Texas, USA [79]. The VAST treatment is actually a combination of mechanical and chemical treatments, where the adherend surface is blasted with a slurry containing fine abrasive particles, e.g., alumina in fluorosilicic acid. The VAST treatment produces an anatase form of oxide on the Ti-6Al-4V alloy that is stable up to 175°C but converts to the rutile form when heated to higher temperatures [79]. The durability of the VAST surface pretreated titanium adherend in 100% relative humidity and 60°C for a period of 2 months was equivalent to that for adherends prepared using phosphate fluoride or modified phosphate fluoride treatments [81, 83].

2.2.7 Chromic Acid Anodizing

The most common anodization pretreatment for titanium is chromic acid anodization (CAA), developed by Boeing [77]. CAA produces a microscopically rough oxide morphology on the Ti-alloy surface, which enhances bond durability. The microscopically rough surface produces a greater degree of mechanical interlocking between the adherend and the adhesive. The adherend surface roughness, of the order of tens of nanometers, plays a major role in enhancing bond durability [69, 84].

Anodization is usually carried out at a relatively low voltage, usually 5 volts; anodization at higher voltage tends to produce oxide coatings that are brittle [77,85]. The anodization procedure is given in the experimental section of this dissertation. The chemical and physical nature and stability of the oxide coatings are discussed in great detail in section 2.4.

2.2.8 Plasma Treatment

Plasma treatment of polymer, metal or composite surfaces results in the production of functional groups on these surfaces which improve the wetting properties of polymers, composites and

metals, and increases the chemical interaction between the polymer/metal, polymer/composite and polymer/polymer surfaces [86]. The plasma treatment of adherends improves the wettability of the materials by introducing polar groups on the surface [87-92] by promoting hydrogen bonding [93-95] and by modifying weak boundary layers [96,97]. The plasma surface pretreatment is an environmentally benign and safe technology. Unlike chemical treatments, the plasma treatment does not produce any chemical waste that could be harmful to the environment.

The plasma treatments for adhesive bonding can be classified into two main groups; 1) gas plasma treatment for metal or composite adherends [86] or for polymer coatings [98-100] and 2) plasma-sprayed deposition of organic polymeric [102,103] and inorganic materials [104] onto the adherends. The gas plasma treatment of adherends usually involves treatment with plasmas of gases such as oxygen, nitrogen, argon, ammonia, or dry air.

Plasma-sprayed Ti-6Al-4V coatings have been used as a surface pretreatment for Ti-6Al-4V [7, 101]. A thin microscopically rough oxide morphology was produced when Ti-6Al-4V was plasma sprayed on Ti-6Al-4V adherends. The bond durability of plasma-sprayed adherends maintained in a hot-wet environment (60°C and 95% relative humidity) was comparable to the performance of adherends treated with common chemical and electrochemical treatments, with bond failure taking place entirely in the adhesive [101]. The durability of plasma-sprayed Ti-6Al-4V adherends, bonded with a FM-300M epoxy, and tested in boiling water was comparable to that for adherends treated via CAA and SHA [7]. Compared to non-thermally treated plasma-sprayed adherends, plasma-sprayed Ti-6Al-4V adherends exposed to 450°C in vacuum for different times (up to 165 hours) prior to adhesive bonding, showed no significant reduction in the tensile strength [7]. The plasma-sprayed specimens always failed cohesively within the adhesive. In contrast, tensile strength was reduced significantly and bond failure occurred entirely in the oxide coatings when a CAA treated adherend was exposed to 450°C in vacuum for as little as 3 hours prior to adhesive bonding. The superior performance of plasma sprayed adherends vs. CAA treated adherends was attributed to the presence of a relatively thin native oxide coating on the plasma-sprayed adherend compared to a much thicker oxide coating on the

CAA treated adherend. For a plasma-sprayed adherend, it was suggested that complete dissociation of a thin native oxide coating upon exposure to high temperature allows the adhesive to interact via mechanical keying and to form chemical bonds directly with the plasma-sprayed Ti-6Al-4V coatings. By comparison, dissociation of CAA oxide coatings results in the dissolution of oxygen in the Ti-6Al-4V alloy and the formation of an embrittled region in the alloy.

The durability of aluminum and titanium adherends plasma-sprayed with inorganic materials and bonded with a polyimide adhesive was studied by Wolfe et al. [104]. The durability of bonded specimens was evaluated using a cyclic environment exposure scheme including low temperature (-20°C), hot-wet conditions (70% R.H. at 66°C), high temperature (160°C) in air, high temperature (160°C) in vacuum (130 torr, 0.2 atm.), and room temperature. The durability of aluminum adherends plasma-sprayed with Al₂O₃, AlPO₄, MgO and SiO₂ was comparable with that for phosphoric acid anodized (PAA) aluminum adherends. The bond durability of Ti-6Al-4V adherends plasma-sprayed with TiO₂, TiSi₂, MgO and SiO₂ inorganic coatings was comparable with that for Turco surface pretreated Ti-6Al-4V adherends.

Plasma-sprayed polymer coatings as a surface pretreatment for titanium were characterized by Dillard and co-workers [102,103]. The durability of titanium, plasma-sprayed with polyimides, bonded with a glass supported FM-5 adhesive, and tested in boiling water was investigated [102]. The adherend surfaces were plasma sprayed with polyimides namely, LaRC TPI-2000, LaRC PETI-5, Aurum PD 400, and Aurum PD 450. The plasma-sprayed polymeric coatings retained their principal chemical characteristics, i.e., no detectable degradation of the plasma sprayed polymeric material resulting from plasma-spraying, per se, was observed. The durability of LaRC TPI-2000/Ti and LaRC PETI-5/Ti bonded joints tested in boiling water was comparable to that for joints prepared using CAA surface pretreated titanium. The Aurum/Ti bonded joints were not as durable as CAA surface pretreated bonded joints. The durability of titanium and aluminum adherends plasma-sprayed with polymer materials such as epoxy, polyester, polyimide and cyanate ester and their mixtures, and bonded with either a FM-36 polyimide film or a AF-191 epoxy film were studied by Dillard et al. [103]. The titanium or aluminum adherends plasma-

sprayed with bis-maleimide/cyanate ester mixture or a bis-maleimide/LaRC TPI-1500 mixture and bonded with a AF-191 epoxy or a FM-36 adhesive film and exposed to an environmental cycle, exhibited durability better or comparable to that for PAA treated aluminum adherends or Turco treated titanium adherends.

2.3 Titanium Alloy (Ti-6Al-4V)

Titanium and its alloys have excellent thermal stability, creep resistance, superior corrosion resistance, and a high strength-to-weight ratio which makes titanium a suitable construction material for aerospace applications. Titanium metal and steel are equally strong, but titanium is 45% lighter than steel [105]. Also, titanium metal is 60% heavier than aluminum, but is twice as strong [105].

Ti-6Al-4V alloy is an α - β phase alloy (dimorphic), which retains a high fracture toughness and strength at temperatures up to 399°C (750°F). The alloying elements, aluminum and vanadium are α (alpha) and β (beta) - phase stabilizers, respectively [106]. The β -phase has a body-centered cubic structure and the α -phase has the hexagonal close-packed structure. The Ti-6Al-4V alloy is an excellent material for high performance structures because α - β alloys show good cold and hot strength [107] in addition to good formability.

2.4 Anodic oxide coatings of Ti-6Al-4V alloy and their hygro-thermal stability

Chromic acid anodization (CAA) is an excellent surface pretreatment for titanium alloys for adhesive bonding. CAA produces a microscopically rough multilevel oxide morphology on the Ti-alloy surface which enhances bond durability [7]. The multilevel morphology of the CAA oxide coating is the result of differential etching rates for α (alpha) and β (beta) phases of the Ti-6Al-4V alloy. The surface macro-roughness of the anodic oxide coating is of the order of 2.1 μm [68]. At the microscopic level, the oxide coatings have a porous, columnar and cellular structure. The oxide coating has a thin (8-15 nm) barrier oxide layer at the bottom of the columnar

structure. The pore diameter in the anodic oxide columns is about 40 nm [8,108]. The mechanism of pore formation is not well understood, but hydrofluoric acid is believed to play a major role in the formation of the porous oxide structure [109]. A thinner, smooth and compact oxide coating was obtained when hydrofluoric acid was not added to the anodizing solution [109]. Skiles and Wightman, showed that a relatively thinner oxide coating, about 20 nm thick, is produced when Ti-6Al-4V is anodized without hydrofluoric acid and a relatively thicker oxide coating, about 140 nm, is produced when anodized in the presence of hydrofluoric acid [108]. Kover and Musselin studied the growth mechanism of anodic oxide coatings and found that oxide growth takes place primarily due to the migration of metal cations through a stationary oxygen sublattice [110]. The thickness of the anodic oxide coating is proportional to the applied voltage [111], and the oxide coating thickness is about 40 nm when anodized at 5 Volts and about 80 nm when anodized at 10 Volts for 20 minutes [112]. The chromic acid anodization solution composition, anodization time and anodization solution temperature are some of the other variables that influence the thickness of the anodic oxide coating [108]. All other anodization variables being the same, an increase in anodization time from 20 minutes to 60 minutes resulted in an increase in oxide thickness from 140 nm to about 290 nm when anodized at 10 Volts [108]. Also, decreasing the anodization solution temperature resulted in a non-linear increase in the oxide thickness [108]. The porous, columnar and cellular structure of the oxide coatings offers the possibility for deeper penetration by adhesives and primers [70], resulting in a greater degree of mechanical keying between the adhesive and adherend. The CAA oxide coating is amorphous [113,114], and has a bulk composition of TiO_2 . The CAA oxide on Ti-6Al-4V is acidic with a surface oxide pH in the range of 1.2 to 3.4 [68].

The oxide coating on CAA surface treated Ti-6Al-4V is chemically very stable under ambient exposure conditions, but when exposed to elevated temperatures [7,8] or humidity [115] or hot water [116,117], undergoes chemical and/or morphological changes. The morphological and/or phase transformation in the CAA oxide coating may produce internal stresses. The stressed oxide coatings are susceptible to stress induced cracking and could fail under minimal applied

load. Such environmentally induced chemical and physical transformation of CAA oxide coatings could affect the durability of a bonded joint [69].

When exposed to a hot-wet environment, the amorphous titanium dioxide (TiO_2) coating on a CAA treated Ti-6Al-4V converts to a crystalline anatase form (a tetragonal form of TiO_2) [114,116]. The formation of a crystalline phase and a change in the morphology of the CAA oxide was not accompanied by any chemical transformation. The presence of water influences the temperature at which the phase transformation takes place in the oxide of a CAA treated Ti-6Al-4V [116]. In a low humidity (R.H. \cong 0) atmosphere at 100°C , the CAA oxide retains its amorphous nature even after 100 hours of exposure. When a CAA Ti-oxide is exposed to water at 85°C for more than 20 hours, the amorphous titanium dioxide (TiO_2) changes to a crystalline anatase phase. By contrast, in a similar environmental exposure condition, the FPL and PAA oxide coatings on aluminum adherends become hydrated in 2 minutes and 3 to 5 hours, respectively [69]. Thus, oxide coatings on CAA treated Ti-6Al-4V adherends are relatively more stable chemically than the PAA and FPL oxide coatings on aluminum adherends in a hot-wet environment.

M. Assefpour-Dezfuly et al. studied the stability of CAA oxide coatings on commercially pure titanium in the presence of water [117]. The oxide coating on a CAA treated commercially pure titanium adherend was uniform and porous, and the oxide morphology was similar to that of a CAA treated Ti-alloy (Ti-6Al-4V). The oxide morphology of a CAA treated commercially pure titanium remained unchanged when immersed in de-ionized water at 80°C for 100 hours, the amorphous oxide was not converted to the crystalline anatase form. This result was in sharp contrast to the work of Natan and Venables, where the amorphous oxide coating on a CAA treated Ti-6Al-4V alloy converted to the anatase form under a similar environmental exposure condition [116]. This difference in morphological effects of oxide hydration between the oxides of a CAA treated commercially pure titanium and the oxides of a CAA treated Ti-alloy (Ti-6Al-4V) could be due to the presence or absence of alloying elements in the adherends. However, when a CAA treated commercially pure titanium specimen was immersed in tap water at 80°C

for 100 hours, the titanium oxide surface was covered with numerous small leaf-shaped crystals. The chemical and morphological nature of the leaf-shaped crystals was not identified. However, the appearance of the leaf-shaped crystals was similar to that of the anatase crystal form observed by Natan and Venables [116]. It was suggested, that the presence of dissolved salts in exposure medium (tap water) could be responsible for crystal formation on the surface of CAA treated pure titanium.

The characteristic micro-rough oxide morphology was retained when CAA treated Ti-6Al-4V adherends were exposed to 330°C in air for up to 1200 hrs and at 450°C in vacuum for up to 160 hrs [8]. Air exposure resulted in only a slight thickening of the CAA oxide cell walls. The characteristic CAA oxide morphology was lost to some extent when CAA Ti-6Al-4V was held at 500°C in vacuum, and was completely lost when maintained at 700°C for 1 hour [7]. The work of Clearfield and co-workers indicated that the oxide coatings prepared via CAA become chemically unstable when exposed to temperatures above 330°C in air or in vacuum [7]. Clearfield and co-workers observed a significant tailing of the oxygen signal (the oxide/metal interface was not sharp) in AES depth profile measurements for a thermally treated (450°C for 1 hr or 700°C for 1 hr, in vacuum) CAA anodized Ti-6Al-4V alloy. A similar tailing of the oxygen signal was observed in AES depth profile data for thermally treated (500°C for 1 hr, in vacuum) SHA and Pasa-Jell 107 surface treated Ti-6Al-4V adherends. The oxygen concentration immediately below the surface was near the solubility limit (25 atomic percent) in the alloy. It was suggested by Clearfield and co-workers that during thermal treatment of a CAA - Ti-6Al-4V adherend oxygen diffuses from the oxide (oxide dissociation) into the alloy (oxygen dissolution) and forms a brittle zone in the alloy near the metal/oxide interface. Dissolution of oxygen into the titanium alloy at concentrations as low as 0.1 to 1.0 atomic percent results in the formation of an embrittled zone (reduced fracture toughness) just below the oxide/metal interface [118,119]. Further the dissociation of the oxide and its subsequent dissolution into the alloy would result in the formation of weak nonstoichiometric oxides which have defects. Therefore, the formation of an embrittled zone just under the alloy/oxide interface and weakening of the oxide coatings could

cause thermally treated ($>300^{\circ}\text{C}$) adhesively bonded joints to fail in the embrittled zone and/or in the oxide coatings under a minimal load.

The anodic oxide coatings on Ti-6Al-4V adherends are also produced via sodium hydroxide anodization (SHA) [58,120,121]. The SHA oxide coatings have a high degree of surface roughness and porosity which are similar to the CAA oxide coatings. The SHA oxide coatings on Ti-6Al-4V are basic with a surface pH greater than 8.0 [58].

2.5 Durability of Adhesively Bonded Titanium

Since most adhesively bonded joints may eventually encounter a hot and/or humid environment, studies involving the influence of temperature and water on the durability of adhesively bonded joints are of paramount importance. The combined effect of water and temperature could immensely reduce the integrity of an adhesively bonded joint. In general, the modulus, strength and glass transition temperature of the adhesive film decrease due to the presence of water in the adhesive [122]. Water ingress in the adhesive could result in plasticization of adhesive, causing a decrease in strength [123]. However, in some instances, the presence of water results in an improvement in the adhesive performance, for example, the toughness of an adhesively bonded joint increased initially when exposed to moisture [124]. This initial increase in toughness is attributed to a decrease in the adhesive's yield strength at the crack-tip and blunting of the crack-tip due to plasticization of adhesive in the crack-tip area by water molecules. Adhesively bonded joints could fail in the presence of water due to delamination of the adhesive film. For example, water attacks the epoxy/titanium interface causing the delamination of the adhesive film leading to ultimate failure of the bond [125]. Water could attack and chemically transform the interfacial metal oxide coating thereby weakening the adhesive/adherend interface [116]. Some of the important effects of moisture/water on a adhesively bonded joint are summarized below:

- Water could cause plasticization of the adhesive, which in general weakens the adhesive.

- Water could displace adhesive from the high free energy substrate surface where adhesive/adherend interaction is in the form of weak van der Waals' forces
- Water could attack and degrade the oxide on the adherend surface
- Water could chemically degrade the adhesive by hydrolysis. Structural adhesives are in general highly resistant to hydrolysis, but depending on the nature of chemical groups in the adhesive and the chemical nature of the exposure media and temperature, hydrolysis of the adhesive is a possibility
- Water could break the chemical bonds between adherend and adhesive.
- Water could cause swelling of the adhesive when absorbed in large amounts and thus introduce large amounts of internal stresses.

In moderate environments (60°C, 95% RH), the microscopically rough oxide morphology on Ti-6Al-4V adherends provides the best overall durability [120,126-129].

The influence of different surface pretreatments on bond durability of Ti-6Al-4V alloy, bonded with an epoxy film, in a combination of hot and dry or wet environments was evaluated [121]. The three different surface pretreatments used for preparing titanium alloy surfaces were alkaline hydrogen peroxide etch (AHP), sodium hydroxide anodization (SHA) and catalytic alkaline hydrogen peroxide etch (CAHP). The three surface pretreatments, AHP, SHA and CAHP produced equally durable titanium/epoxy bonded joints [121].

The influence of four different surface pretreatments, chromic acid anodization (CAA), sodium hydroxide anodization (SHA), phosphate fluoride acid etch (P/F) and TURCO basic etch, on the bond durability of Ti-6Al-4V alloy/epoxy bonded joints in a hot/wet environment was evaluated using a Boeing wedge test and a single lap shear test [70]. An unsupported FM-300U epoxy adhesive film was used for adhesive bonding. From the Boeing wedge test, SHA and CAA pretreated titanium joints were equally durable in 80°C, 95% relative humidity, while the TURCO pretreatment was slightly less durable. P/F surface pretreated titanium exhibited the least durability under such environmental exposure condition. However, measured lap shear

strengths for CAA, P/F, and TURCO surface treated titanium adherends were not significantly different.

The durability of SHA/titanium adherends, bonded with a FM-300 structural epoxy adhesive, and tested in a hot-humid atmosphere (80°C/95% R.H.) and in a 80°C water was evaluated using the Boeing wedge test [58]. The durability of SHA/titanium was comparable to that for CAA surface treated titanium adherends.

Parvatareddy studied the durability of CAA treated Ti-6Al-4V adherends bonded with FM-5 polyimide adhesive. Samples were aged at 150°C, 177°C and 204°C in three different environments; ambient atmosphere, and reduced air pressures of 2 psi and 0.2 psi [130]. Boeing wedge test and double cantilever beam test (DCB) geometries were utilized for evaluating Ti-6Al-4V/FM-5 bond durability. The adhesively bonded joints were aged for up to 18 months in each environment. Adhesively bonded specimens aged at 204°C in an ambient atmosphere performed poorly and showed a drop of 40% in fracture toughness. The loss in fracture toughness was attributed to a combination of physical and chemical aging of the FM-5 adhesive resin.

The influence of various surface pretreatments on the durability of adhesively bonded titanium joints was investigated by Clearfield and co-workers [7]. The four different surface pretreatments for preparing titanium alloy surfaces were SHA, CAA, PS, and grit blast. The adherends were bonded with a FM-300M adhesive. The wedge test results for specimens immersed in boiling water show that titanium treated with the surface pretreatments, SHA, CAA, and PS produced equally durable titanium/epoxy bonded joints. The grit-blasted adherends performed poorly. The crack propagation in CAA treated specimens was entirely within the adhesive, and it was at the adhesive/adherend interface for SHA, PS, and grit-blast treated adherends. The difference in failure mode for CAA and SHA treated specimens was attributed to the contribution to bonding from acid-base interaction (between oxides and adhesive) in CAA treated specimens and its absence in the SHA treated specimens.

CAA treated Ti-6Al-4V adherends show poor bond durability when exposed to high temperatures [7,8,131]. The influence of a thermal treatment on the tensile strength of Ti-6Al-4V alloy/epoxy bonded joints was investigated as a function of surface pretreatment [8]. As anodized SHA and CAA adherends exhibited similar tensile bond strengths and failed cohesively within the adhesive. However, when exposed to hot air or vacuum, unlike CAA treated specimens, the SHA treated specimens retained most of their initial strength. Also, unlike CAA treated specimens, the SHA treated specimens retained much of their initial strength following exposure to 250°C and 350°C steam (water vapor), and bond failure was cohesive within the adhesive.

The role of surface preparation on the tensile bond-strength of Ti-6Al-4V/FM-300M joints subjected to high temperature environment was investigated by Clearfield and co-workers [7]. The four different surface pretreatments for preparing titanium alloy surfaces tensile tests were CAA, SHA, PS (plasma-sprayed), and Pasa-Jell (PJ 107). For tensile bond strength measurements, surface treated adherends were bonded to an aluminum fixture with a room temperature curing epoxy (3M 1838) adhesive. The CAA and SHA treated Ti-6Al-4V adherends were thermally treated either in air at 330°C for various times up to 1200 hr or in vacuum at 400°C for various times up to 160 hr. The as anodized CAA and SHA surface treated specimens exhibited similar tensile strengths. However, when exposed to 330°C for 160 hours in air prior to adhesive bonding, the SHA surface treated specimens lost only about 25% of their initial strength compared to a loss of nearly 60% of their initial strength for the CAA treated specimens. In each case, the failure mode was mixed-mode, i.e., failure was partially within adhesive and partially within the oxide coating. When thermally treated in vacuum at 400°C for 24 hours or 450°C for 3 hours prior to adhesive bonding, the CAA treated specimens lost almost all of their initial tensile bond strength and failure was entirely in the oxide coating. In contrast, when exposed to 400°C for 24 hours in vacuum prior to adhesive bonding, the SHA treated specimens still retained about 50-60% of their initial tensile bond strength and failure was mixed-mode. Bond failure at the metal/oxide interface was attributed either to stress buildup at the metal/oxide interface or to a change in the alloy microstructure [8]. However, later studies suggested that the failure in the

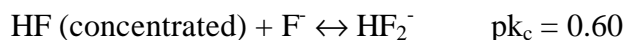
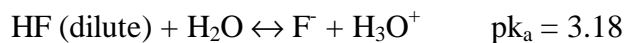
oxide was due to dissociation of the oxide and subsequent diffusion of oxygen into the alloy, which weakened the interface [7]. The tensile strength of PJ treated titanium specimens was less than the as anodized CAA and SHA specimens, and the bond failure mode was mixed-mode. The PJ treated specimens lost almost 75% of their initial strength when exposed to 200°C in vacuum for 1 hour, and failure occurred in the oxide. In sharp contrast to electro-chemical surface pretreatments, the plasma-sprayed Ti-6Al-4V specimens retained almost 90% of their initial strength when exposed at 450°C in vacuum for up to 165 hours prior to bonding, and failure was always cohesive within the adhesive.

In durability studies, SHA treated titanium performed better than CAA/titanium when exposed to high temperatures [131-135]. The SHA/titanium adherends when exposed to high temperatures and a dry environment did not lose as much strength as CAA treated titanium adherends over a similar exposure time [132,133]. However, when SHA/titanium adherends, bonded with a polyimide adhesive, were aged at 232°C for greater than one year, a dramatic decrease in bond strength and bond failure in the oxide coating was observed [131,134,135]. The CAA treated titanium adherends bonded with a polyimide adhesive lost most of their lap shear strength after about 8000 hours of exposure whereas SHA treated titanium adherends lost strength after about 13,000 exposure hours [134].

2.6 Fluoride ions in oxide coatings: thermodynamic considerations of their reactivity with the alloying metals and their oxides

The chemical nature of fluoride ions in the oxide coatings of CAA treated Ti-6Al-4V alloy is not well established. Fluoride ions could be present as adsorbed anions [17] and/or could be present in the metal oxide lattice as a substitute (impurities) for O^{2-} ions. Since F^- and O^{2-} anions have very similar ionic radii [18], the substitution of F^- anions for O^{2-} ions in the metal oxide lattice is common [19,20]. Fluoride ions could be associated with hydrogen in the form of hydrofluoric acid since metal oxides in general retain some amount of moisture when exposed to the

atmosphere at ambient temperature [16]. The chemical equilibrium reactions between water, hydrofluoric acid, fluoride ion, and hydronium ions are shown below [136].



The fluoride ions in the CAA oxide coatings could react with the metal oxides and/or with the constituent metals of the Ti-6Al-4V alloy to form metal fluorides and/or metal oxyfluorides or other reaction products. Table 2.1 lists some of the possible chemical reactions of hydrofluoric acid with the metals and their oxides. The standard Gibbs free energy of reaction was calculated from published data for standard free energies of formation for reactants and products involved in the chemical reactions. The standard Gibbs free energies of reaction ($\Delta_r G^\circ$) at room temperature (298.15°K) and at high temperature (700°K) are summarized in Table 2.1. The published values for $\Delta_f G^\circ$ for titanium oxide, aluminum oxide, titanium fluorides, aluminum fluoride, water and hydrofluoric acid at room temperature (298.15°K) and at 700°K are listed in Table 2.2 [137-139].

Except for chemical reaction involving vanadium oxide, all other chemical reactions have a negative standard $\Delta_r G^\circ$ at room temperature, suggesting a spontaneous reaction at room temperature. The chemical reaction between titanium dioxide (TiO₂) and vanadium with hydrofluoric acid at room temperature has a small negative standard $\Delta_r G^\circ$ but at 700°K has a positive standard Gibbs free energy of reaction. The positive value of $\Delta_r G^\circ$ suggests that at least thermodynamically, the reaction between titanium dioxide and hydrofluoric acid to form titanium tetrafluoride and water is not likely at around 700°K. Similarly, based on thermodynamic considerations alone, the reaction between vanadium oxide and hydrofluoric acid to form

Table 2.1. Equilibrium chemical equations and calculated standard Gibbs free energy of reaction ($\Delta_r G^\circ$) values at room temperature (298.15°K) and at 700°K.

Chemical Reactions	$\Delta_r G^\circ$ (reaction) at 298.15°K, kJ	$\Delta_r G^\circ$ (reaction) at 700°K, kJ
$2\text{Al (s)} + 6\text{HF (g)} \rightarrow 2\text{AlF}_3 \text{ (s)} + 3\text{H}_2 \text{ (g)}$	-1214.6	-990.0
$\text{Al}_2\text{O}_3 \text{ (s)} + 6\text{HF (g)} \rightarrow 2\text{AlF}_3 \text{ (s)} + 3\text{H}_2\text{O (l)}$	-343.6	-160.3
$2\text{Ti (s)} + 6\text{HF (g)} \rightarrow 2\text{TiF}_3 \text{ (s)} + 3\text{H}_2 \text{ (g)}$	-1076.2	-869.4
$\text{Ti (s)} + 4\text{HF (g)} \rightarrow \text{TiF}_4 \text{ (s)} + 2\text{H}_2 \text{ (g)}$	-460.8	-335.8
$\text{TiO}_2 \text{ (s)} + 4\text{HF (g)} \rightarrow \text{TiF}_4 \text{ (s)} + 2\text{H}_2\text{O (l)}$	-45.6	+62.5
$\text{Ti}_2\text{O}_3 \text{ (s)} + 6\text{HF (g)} \rightarrow 2\text{TiF}_3 \text{ (s)} + 3\text{H}_2\text{O (l)}$	-353.7	-175.3
$2\text{V (s)} + 10\text{HF (g)} \rightarrow 2\text{VF}_5 \text{ (g)} + 5\text{H}_2 \text{ (g)}$	-1.0	+192.4
$\text{V}_2\text{O}_5 \text{ (s)} + 10\text{HF (g)} \rightarrow 2\text{VF}_5 \text{ (g)} + 5\text{H}_2\text{O (l)}$	+232.8	+395.1

Table 2.2. The published standard Gibbs free energy of formation ($\Delta_f G^\circ$) values for titanium oxide, aluminum oxide, titanium fluorides, aluminum fluoride, water and hydrofluoric acid at room temperature (298.15°K) and at 700°K.

Chemical Compound	($\Delta_f G^\circ$) at 298.15°K (kJ/mol) *	($\Delta_f G^\circ$) at 700°K (kJ/mol) *
TiO ₂ (s)	-889.4	-815.9
Ti ₂ O ₃ (s)	-1433.8	-1320.5
V ₂ O ₅ (s)	-1419.3	-1246.7
Al ₂ O ₃ (s)	-1582.3	-1456.1
AlF ₃ (s)	-1431.1	-1326.3
TiF ₃ (s)	-1361.9	-1266.0
TiF ₄ (s)	-1559.2	-1444.2
VF ₅ (g)	-1373.5 ^{\$}	-1289.3 ^{\$}
HF (g)	-274.6	-277.1
H ₂ O (l)	-237.1	
H ₂ O (g)		-208.8

- M.W. Chase Jr., C.A. Davies, J.R.D. Downey Jr., D.J. Frurip, R.A. McDonald and A.N. Syverud, Eds., JANAF Thermochemical Tables, 3rd edition, American Chemical Society, Washington D.C., Vol. 14, No. 1, 1986.

^{\$} Thermochemical Data of Pure Substances, ed. Ishan Barin, VCH Publishers, Inc., New York, NY, USA, 3rd edition, 1995.

vanadium pentafluoride (VF_5) is not likely to take place between 298.15°K (room temperature) and 700°K. Also, thermodynamically the reaction between vanadium and hydrofluoric acid to form vanadium pentafluoride is not feasible above room temperature.

Based on thermodynamic considerations alone, fluoride in the form of hydrofluoric acid is expected to attack the CAA oxide coatings and the underneath metal (if possible), to form aluminum trifluoride (AlF_3), titanium trifluoride (TiF_3) or titanium tetrafluoride (TiF_4) in the temperature range 298.15°K to 700°K. However, for any chemical reaction to take place, the reaction should not only be thermodynamically favorable but kinetically favorable. The reaction kinetics may be influenced by many factors, most importantly by temperature, pressure and or concentrations of reactants and products. Even though, some of the above reactions are thermodynamically favorable, it is possible that a reaction may not take place at any appreciable rate at room temperature, because the reaction may involve a large energy barrier (higher activation energy). For example, although the reaction between aluminum oxide and hydrofluoric acid is thermodynamically favorable at room temperature, the industrial production of aluminum fluoride (AlF_3) is carried out by a dry process, where Al_2O_3 is treated at high temperature (500°C to 600°C) in a continuous stream of gaseous hydrofluoric acid [140].

Some of the reaction products listed in Table 2.1 are unstable at room temperature and a few others are unstable at elevated temperatures. In general, metal halides vaporize at a vapor pressure of about 10^{-4} atm unless an equilibrium vapor pressure is attained in a static or recirculating halogen atmosphere [141]. It is worth noting that vanadium fluorides, VF_5 and VF_2 , are highly volatile at room temperature. The vapor pressure of VF_5 is 10^{-2} atmospheres at -17°C [141]. The melting point of VF_5 is 19°C [141]. The vapor pressure of TiF_4 is 10^{-4} atmospheres at 108°C and 1.0 atmosphere at 284°C (sublimation temperature) [141]. The melting point and boiling point of TiF_3 are 1200°C and 1400°C , respectively [141]. The vapor pressure of aluminum trifluoride (AlF_3) is 10^{-4} atmosphere only at approximately 1145°C [141]. Aluminum trifluoride (AlF_3) sublimates at 1291°C [105] and is stable at room temperature.

2.7 Thermal Stability of Polyimide Adhesives

The demand for high performance adhesives which can withstand temperatures in excess of 371°C, and/or are able to maintain thermal stability at 177°C, in air, for more than 60,000 hours [142], has led to the development of a variety of high performance polyimide adhesives for aerospace applications. Thermoplastic and thermosetting polyimides having high toughness and thermo-oxidative stability at elevated temperature have been synthesized [143-146]. For applications requiring excellent resistance to high temperature and harsh environments, the aromatic class of polyimides is among the most widely studied [146].

The thermal stability of polymers is related to their molecular structure. The presence of heterocyclic imide units in the polymer backbone is mainly responsible for high temperature stability. Polyimides having only aromatic groups in their structure are thermally more stable than polyimides containing aliphatic groups also. For example, the thermal decomposition temperature (t_d) for aromatic polypyromellitimides is higher than the polypyromellitimides containing aliphatic groups [147]. The nature of the diamine structure within a polyimide plays an important role in the thermo-oxidative stability of the polymer. The electron-deficient diamines (relatively less likely site for oxidation reaction) produce more oxidatively stable polyimides than electron-rich diamines [148-150]. The LaRCTM PETI-5 polyimide containing a reactive phenylethynyl end group has a slightly lower thermal stability than the phthalimide endcapped (non-reactive group) LaRCTM -8515 polyimide [151].

The chemical and/or physical changes produced in the polymers due to thermal exposure are monitored by a variety of methods, namely - chemical analysis, spectroscopic methods and thermal analysis [152,153]. In thermal analysis, the isothermal or dynamic weight loss of a polymer is determined in air (thermo-oxidative degradation) and/or in an inert atmosphere (thermal degradation) such as nitrogen. Thermal analysis of the polymer is carried out in a thermogravimetric analyzer and usually the temperature corresponding to a 5% weight loss of the polymer material is determined and reported. A polymer with up to 95% of its original weight

retains enough integrity for most applications, and hence the temperature corresponding to a 5% weight loss is considered a useful criterion for the thermal stability of a polymer.

2.8 Bonding Configurations

The use of an adhesively bonded joint will be meaningful only if the bonded joint lasts for a long time in the given environment. To test the performance of an adhesively bonded joint in any given environment or combination of environments, many standard test methods have been developed. Kinloch has summarized a list of ASTM (American Society for Testing and Materials) and BS (British Standards) standard test methods which are commonly used for assessing the performance of an adhesively bonded joint [154]. In most cases, where the adhesively bonded joint is expected to last for a long time, it is impractical to conduct the performance evaluation test for a period equal to or exceeding the bonded joint's life expectancy, and hence short duration (accelerated) tests are performed. The accelerated tests are performed primarily for two reasons, first, to be able to predict the life of a bonded joint without having to perform actual life-time tests and second, to be able compare and evaluate the performance of different variables utilized in the construction of a bonded joint. The bonded system must be modeled accurately, i.e. all parameters affecting the bonded joints must be established to predict long term durability based on short term tests. The long term durability prediction based on accelerated test data is not a very mature science due to the complex nature of the behavior of different parameters. However, accelerated tests could be carried out to evaluate the relative influence of different variables on performance, such as, adhesive, surface pretreatment, primer etc., used in the construction of the bonded joint. Standard tests have been developed that allow a meaningful comparison of bond durability data for different combinations of bonded joint/environmental conditions.

Different mechanical tests have been employed to evaluate the performance of adhesively bonded joints [155,156]. Most of the mechanical tests are destructive in nature, and each has its own advantages and disadvantages. Depending on the geometry of the bonded joint and loading

conditions, the adhesively bonded joint is subjected to a variety of different stresses. The four most common stress-types to which adhesively bonded joints are subjected in a real world application, are illustrated in Figure 2.1. The in-plane shearing or sliding (mode II), normal stress, out-of-plane shearing or tearing (mode III), opening or cleavage (mode I) and peel. In most mechanical test methods mode I and mode II are the dominant stresses [157].

2.8.1 Single Lap Shear Test Geometry

The single lap shear (SLS) test geometry is the most widely used test geometry for evaluating the performance of adhesively bonded joints. The test is conducted in accordance with ASTM D1002-72 standards [158]. The test method is popular for two main reasons, first, many of the adhesively bonded joints in industrial applications have the joint geometry of a single lap shear test and second, the stresses in such joints are relatively simple to analyze. Also, the testing procedure is simple and the test specimen is inexpensive to fabricate. The test method is generally used for comparing different surface preparation methods and for studying the environmental durability of adhesives. However, the single lap shear test method suffers from some disadvantages. Due to the asymmetric nature of the test geometry, the stress is concentrated near the overlap edges of bonded joint and is not uniform in the adhesive layer as assumed (refer to Figure 2.2). Therefore, when a test specimen is subjected to tensile loading, the specimen experiences a bending motion in addition to shear. Also, the average shear strength, as determined from the SLS test, is not a unique value characteristic of the adhesive material. The determined average shear strength value of a bonded joint in the SLS configuration is a function of many factors, including, geometry of the joint, thickness of the joint, and adherend material [159]. So, care must be taken in using the average lap shear strength values obtained for the purpose of engineering design of a bonded joint.

2.8.2 Wedge Test Geometry

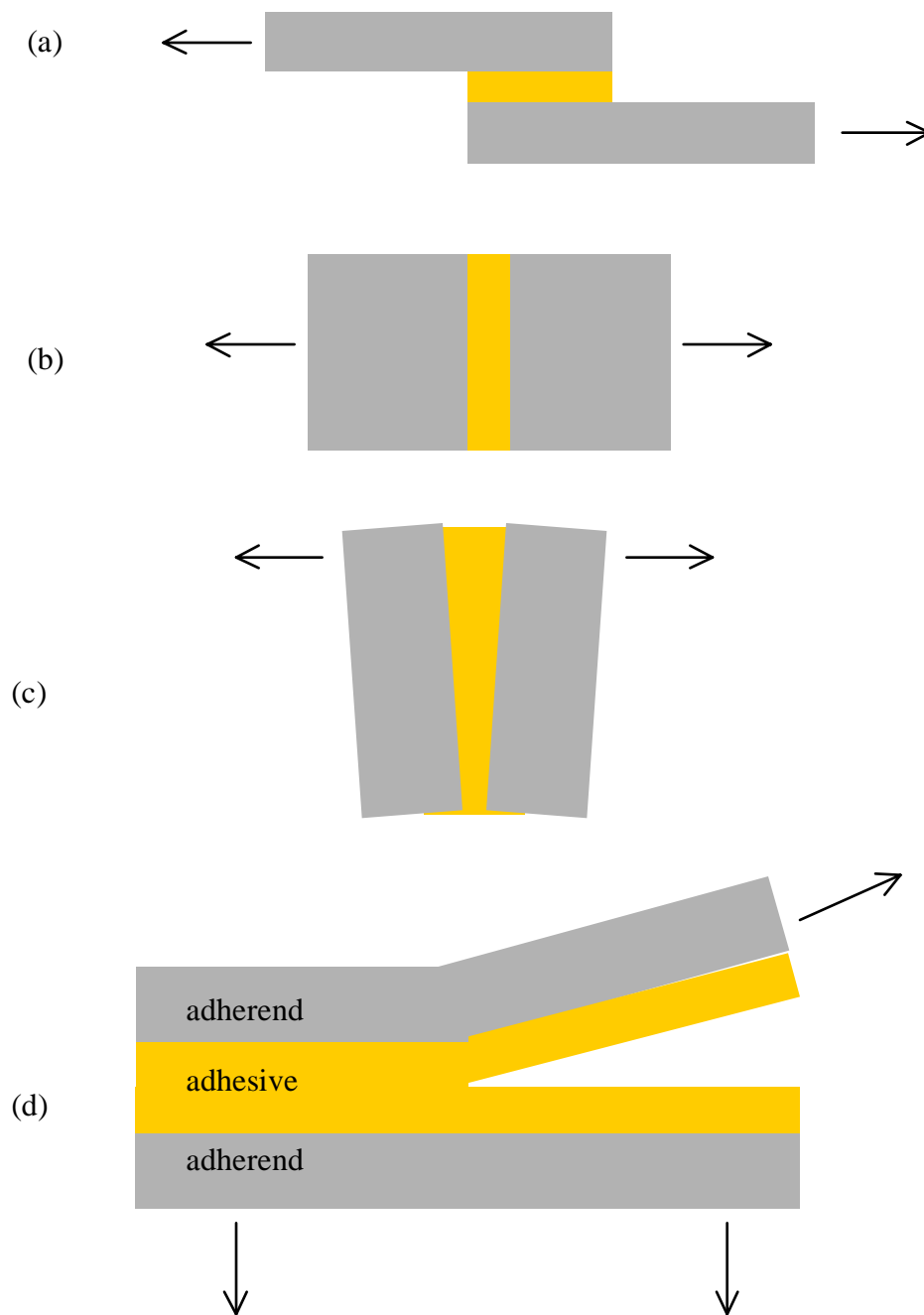


Figure 2.1. The four most common stress-types: (a) shear, (b) normal, (c) cleavage and (d) peel.

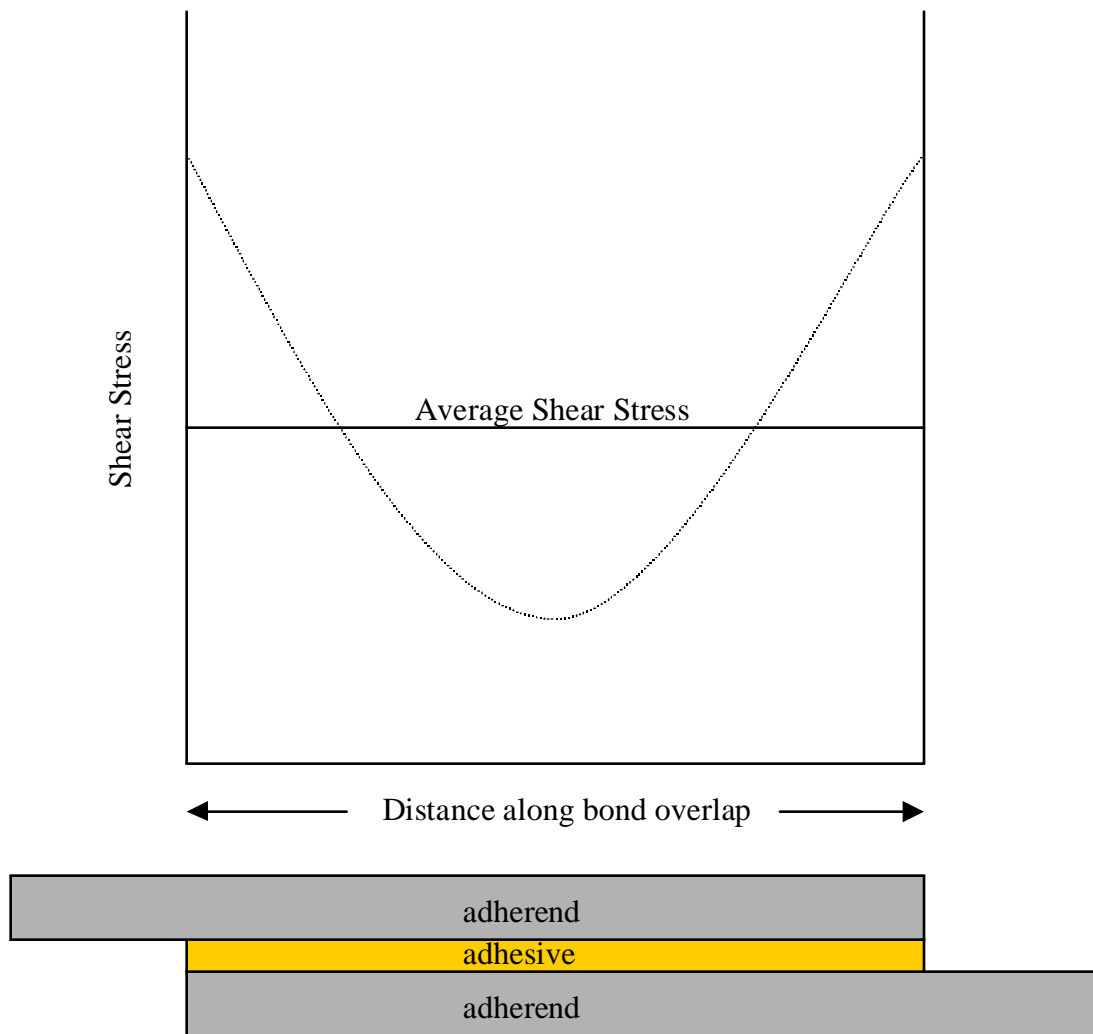


Figure 2.2. A schematic diagram of elastic stress distribution (non-uniform) in the adhesive layer.

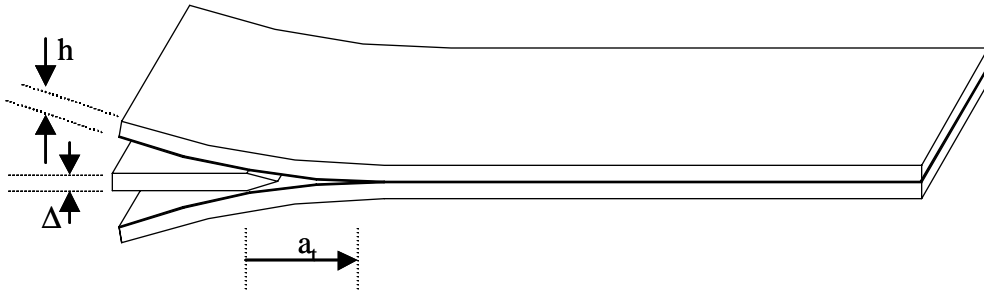
The wedge test, also known as Boeing wedge-test, was developed by Marceau and coworkers [160]. A schematic diagram, showing the typical wedge specimen is given in Figure 2.3. The wedge-test is now a standard testing method (ASTM D 3762) to evaluate the bond durability [161]. The wedge test is a modification of the uniform double cantilever beam test. In the wedge test, a constant displacement is applied to the wedge sample rather than a constant load as applied in the double cantilever beam test. The strain energy release rate (fracture energy), G , can be determined using wedge-tests for specimens subjected to environmental exposure. The Boeing wedge-test is a simple and a very useful test method to study the effects of environment on the durability of adhesively bonded joints [162]. The wedge test geometry was used by Kinloch and coworker to study the influence of three different surface pre-treatments on the durability of aluminum/epoxy joints [163]. Kennedy et al. used the wedge test to investigate the influence of different surface pre-treatments on the durability of titanium/epoxy bonded joints [120]. However, the wedge-test is not a useful test method for adhesively bonded joints where adhesive creeps excessively to remove the stress factor from the test environment by relieving the local stresses. The other disadvantage of the wedge test is that the test specimen must be removed periodically from the test environment to make the crack length measurement, which may not be always convenient or desired especially when the test is carried out in a harsh environment. Also, it is sometimes difficult to locate the crack tip precisely and therefore the crack growth/length is very difficult to measure accurately.

The wedge test geometry allows one to calculate the strain energy release rate (fracture energy), G , of an adhesively bonded joint as a function of crack length [164]. Using two basic assumptions the fracture energy can be calculated using the equation given below [160,162]:

$$G = \frac{3E\Delta^2 h^3}{16a_t^4}$$

Where,

E is modulus of elasticity of the adherend



$$G = 3E\Delta^2h^3/16a_t^4$$

Where,

G = strain energy release rate (fracture energy)

E = modulus of elasticity of the adherend

Δ = thickness of the wedge

h = thickness of the adherend

a_t = crack length at time, t

Figure 2.3. A schematic diagram of a typical wedge specimen.

h is adherend thickness

Δ is thickness of the wedge and

a_t is crack length at time t

The two assumptions are 1) the adherend does not deform plastically and 2) the specimen compliance is primarily due to beam bending and that the contribution to specimen compliance is minimal from the beam shear and adhesive deformation.

As the crack length increases, the strain energy release rate decreases. The strain energy release rate corresponding to a crack arrest (G_{arrest}) is used to evaluate the performance of adhesively bonded joints as a function of adherend surface pretreatment, and/or for comparing performance in various environmental conditions. If crack propagation is in the adhesive then the strain energy release rate (G) is characteristic of the adhesive, and if crack proceeds along the adhesive/substrate interface then G is characteristic of the interface.

2.9 Analytical techniques for material and surface characterization

2.9.1 Fourier Transform Infrared Spectroscopy

There are five basic types of infrared sampling techniques for solid samples; diffuse reflectance, internal reflectance, external reflectance, transmission and photoacoustic spectroscopy. In diffuse reflectance spectroscopy, the externally reflected light, scattered by the sample, is collimated and detected. Diffuse reflectance infrared Fourier transform spectroscopy, DRIFT, is a powerful analytical technique for analyzing powdered and coarse solid samples [165-168]. The DRIFT technique has definite advantages over other infrared spectroscopic techniques due to its non-destructive nature. In cases where it is difficult to grind the sample, the sample surface can be roughened and studied using DRIFT without causing any appreciable damage to the sample.

The Kramers-Kronig transformation [169], a mathematical correction to remove the effects of optical dispersion (dispersion correction) from a reflection spectrum is required in regions of the spectrum that show derivative-shaped bands. The derivative-shaped bands (optical dispersion effects) in a spectrum are the result of variations in the refractive index of the sample. The removal of dispersion effects using Kramer-Kronig transformation, produces a spectrum that closely resembles an absorbance spectrum.

The baseline correction is sometimes necessary to correct a sloping, curving or any undesirable baseline in a spectrum. Since a baseline is that portion of a spectrum where there is no significant reflectance-absorption (ideally, zero absorbance), the baseline correction sets these regions to zero absorbance which otherwise are not at zero absorbance in the original spectrum. There are many factors that result in a non-ideal (tilted, shifted or curved) baseline: some of the major factors are the quality of the background spectrum, sample preparation method and the type of accessory used to obtain the spectrum.

2.9.2 X-ray Photoelectron Spectroscopy (XPS)

The X-ray Photoelectron Spectroscopy (XPS) technique is a powerful surface analytical technique to characterize solid surfaces. This technique is used to obtain the chemical information at the atomic level, from the top 50Å of surface layers. The technique provides information on the elemental analysis and chemical state (oxidation states) of the individual elements in the sample thus the technique provides vital information regarding the chemistry.

In this technique an x-ray is absorbed resulting in emission of electrons from the electronic levels of atoms, the energy of the emitted electrons being characteristic of each element/atom. The kinetic energy (K.E.) of the emitted electron is given by

$$\text{K.E.} = h\nu - \text{B.E.} - \phi$$

where $h\nu$ is the energy of the exciting radiation, B.E. is the binding energy of the emitted electron, and ϕ is the spectrometer work function [170]. Photoelectron emission is probable

when the incident photon energy, $h\nu$, is greater than the ionization energy. The kinetic energy of each emitted photoelectron is measured using an electron spectrometer. The kinetic energy of the photoelectron depends on the energy of the incident radiation. Therefore, a monochromatic x-ray source, such as, Al K_{α} or Mg K_{α} is necessary to obtain high resolution XPS spectra.

In a typical XPS surface analysis, a broad survey scan is performed over a wide energy range, usually between 1 to 1100 eV. The elemental photopeaks are identified based on the characteristic binding energies in the spectrum. The peaks have variable intensities depending on the relative abundance of the different elements and the energy level from which the electron is ejected. Quantitative determination is made using peak height or peak area measurements and applying the sensitivity factor appropriate for the type of analyzer used.

A change in the chemical environment of an atom results in a shift in the core electron binding energies (chemical shift), which is measured directly in XPS. The sensitivity to the chemical environments around the atom is one of the key features of this technique. The chemical shift can result from a change in the nearest neighbor, oxidation-state, compound formation or crystal structure [170]. The shift in binding energies allows bonding and elemental information to be obtained. The binding energies for the various levels of most elements are well known and published [171].

Although this technique is very useful in obtaining chemical information from the solid surface, it suffers some limitations:

- This technique has a poor lateral resolution (1 μ m diameter spot size).
- The elements, hydrogen and helium are undetected because of their low photoelectron emission probability.
- Surface charging, sometimes poses a problem in the interpretation of the XPS spectrum of an insulating solid sample.
- Photo-degradation of materials, especially polymers, due to high-power x-ray beam is a possibility.

- Since the technique is surface sensitive, the sample must be handled very carefully to avoid contamination of the surface from any undesirable sources.

2.9.3 Auger Electron Spectroscopy (AES)

Auger electrons are produced whenever incident radiation in the form of photons, electrons, ions, or neutral atoms interacts with an atom with energy exceeding the amount that is necessary to remove an inner-shell electron (K, L, M, .. etc.) from the atom. The interaction leads to ionization of an atom and creation of a hole in the inner-shell. The ionization process is immediately followed by a de-excitation process where an electron from an outer shell fills in the hole in the inner-shell. Energy is conserved in the de-excitation process either by emission of photons or by ejection of secondary electrons via a radiationless transition. This radiationless transition in which secondary electrons, Auger electrons, are generated forms the basis of Auger Electron Spectroscopy [170]. If the transition involved is between K and L energy levels, then the kinetic energy of the Auger electron is given by,

$$E_a = E_K - E_L - E_L - \phi$$

Where E_K and E_L are the ionization energies of K and L levels and ϕ is the work function of the spectrometer. For Auger radiationless transitions involving specific energy levels, such as KLL, LMM, MNN etc., the kinetic energy of the Auger electron, E_a , is characteristic of the specific element involved in the emission. Since Auger electrons are produced efficiently for orbitals involving lower energies, the lighter elements are detected more easily than the heavier elements. Since Auger spectroscopy requires participation of at least three electrons, the elements, hydrogen and helium are not detected by this method.

In Auger electron spectroscopy, the number of emitted Auger electrons is measured and plotted against the kinetic energy of the electrons. Auger electrons constitute only about 0.1% of total current (electrons) produced during the ionization process. In the presence of a high background backscattered electrons, the identification of Auger peaks from the plot of $N(E)$ vs. K.E.

becomes very difficult [172]. This difficulty is overcome by plotting $d(N)/d(E)$ vs. K.E., where even small signals are easily detected [173].

The Auger electrons of interest have relatively low kinetic energies thus electrons originating from the surface or a few atomic layers below the surface are detected in this technique. The escape depth (depth from which electron escapes the solid without losing energy) is a function of kinetic energy of the electron and to lesser extent a function of the material [174]. Typically, Auger electrons from a depth of 0.5 to 0.3 nm of the surface are detected [175]. Changes in the chemical environment of atoms in the surface region can shift the K.E. and the energy distribution of Auger electrons. The change in energy shifts in Auger spectra can be used to identify the chemical state of surface atoms. Energy shifts are expected whenever a charge transfer takes place from one atom to another. For example, in ionic bonding, the net electron transfer causes core-level electrons of electronegative elements to shift to lower binding energies and those of electropositive elements to shift to higher binding energies. A shift of few electron volts compared to zero valence states is common in such transitions. The spectral shifts in AES are generally more complicated to interpret than XPS peak shifts and are often masked by their large peak widths. On the other hand, the lateral resolution of AES is better than XPS, and for a smaller sampling area, AES is a better choice.

Compositional and depth profiling can be accomplished using AES. Energetic inert gas ions (for example, Ar⁺, from 1 to 5 keV) can be used to sputter the surface. Sputtering is often performed continuously and Auger analysis is conducted in cycles on a set of selected peaks. This type of data acquisition permits analysis at the surface and compositional evaluation at any depth within the film.

This technique also suffers from some limitations:

AES Limitations:

- Elements, hydrogen and helium cannot be detected.

- The primary electron beam used in Auger electron excitation may cause decomposition of the surface materials.
- Quantitative detection sensitivity for most elements is from 0.1 to 1.0 atomic percent.

AES instrumentation typically consists of an electron gun as the primary electron excitation source, an electron spectrometer for energy analysis, a secondary electron detector for imaging, a sample stage for sample manipulation, and an ion gun for sputtering of atoms from the sample surface. Ultra high vacuum of the order of 10^{-7} Torr is required in the chamber where the stage, and electron and ion optical components are housed.

2.9.4 Scanning Electron Microscopy (SEM)

Scanning electron microscopy (SEM) is an important analytical tool to elucidate the morphology/topography of the sample surface. The usefulness of the SEM technique in failure analysis of adhesively bonded structure is enormous. The surface morphology of the failure surface, as determined by SEM, can help understand the failure mechanisms in an adhesively bonded joint. All types of solid samples, insulators or conductors can be studied using SEM. Insulating samples require a thin conducting film, such as gold, on the surface to avoid surface charging during the imaging process. Silver paint is normally used for making an electrical connection between the gold covered surface and the metal mount. A thin conducting metal film on the sample surface and the silver paint as the connector help in reducing the heat related damage to the test sample by efficiently conducting the heat away from the surface [176].

The SEM photomicrograph obtained at an angle normal to the surface, usually provides detailed information about the surface morphology; however, sometimes a 3-dimensional view (stereo image) of the surface is required. The stereo image of the surface is constructed by obtaining photomicrographs of the surface at two different angles and by placing them next to each other and aligning them in such a way that the stereo image is visible using stereoglasses. For stereo images, typically, the difference in angles for the two photographs lies between 5° and 10° [177].

The Energy Dispersive Analysis of X-rays (EDX or EDAX) technique is often used with SEM to make elemental identification of different features in the SEM photomicrographs. In the EDX technique, the energy of X-rays produced by primary electron beam bombardment is measured and used for the identification of elements.

2.9.5 Secondary Ion Mass Spectrometry (SIMS)

In this technique a solid surface is bombarded with a highly energetic beam of ions (primary ions). The secondary ions produced from the solid surface as a result of primary ion bombardment are mass analyzed and detected [178]. The secondary species can be atoms or clusters of atoms, which are neutral, positive or negative ions [179]. However, only charged secondary species (ions) are analyzed by a mass spectrometer yielding a mass spectrum of positive or negative ions. SIMS is capable of better than unit mass resolution depending upon mass spectrometer. The emission efficiency for secondary ions is usually in the range of 0.01 to 1 % of all the emitted species from the surface [180]. Positive ion SIMS spectra are especially sensitive to elements or fragments that form cations (elements on the left side of the periodic table) while the negative SIMS spectra are sensitive to elements or fragments that produce anions (elements on the right side of the periodic table).

SIMS can be used in the static mode to obtain chemical information from the topmost one (monolayer) or two layers of the surface or can be run in a dynamic mode to obtain information from the top several layers of the surface. For SIMS to run in a static mode the primary beam current density should be less than 10 nA/cm² [181]. Since a high sputtering rate is involved in the dynamic mode, dynamic SIMS is not used for any detailed investigation of thin interfacial regions. Dynamic SIMS is usually employed to obtain elemental and isotopic information.

Filbey used SIMS to characterize the oxide coatings on CAA surface pretreated Ti-6Al-4V alloy [68]. Peaks corresponding to titanium isotopes (m/z ratio 46-50) were detected. Among other ions, F^+ at m/z 19 and Al^+ at m/z 27 were also detected.

Gettings and Kinloch successfully used the SIMS technique to investigate the bonding (silane coupling reaction) between γ -glycidoxypropyltrimethoxysilane with mild steel [182] and with stainless steel [34]. Detection of the FeSiO^+ molecular fragment ion in the SIMS analysis of mild steel, and of the CrOSi^+ molecular fragment ion in the SIMS spectra of stainless steel were interpreted to indicate the formation of Fe-O-Si and Cr-O-Si bonds between the silane and the substrate.

2.10 Motivation for the present research work

There are two main reasons for conducting the present research work. First, there is insufficient information on the thermal stability of oxide coatings of CAA treated Ti-6Al-4V adherends in the temperature range, 350°C to 400°C, in air. Second, the influence of the fluoride ion, which is present in oxide coatings of CAA treated Ti-6Al-4V adherends, on the strength and durability of adhesively bonded titanium joints has not been studied.

The thermal stability of oxide coatings is an important consideration in the selection of a suitable surface pretreatment for adherends for adhesive bonding for high temperature applications. Chromic acid anodization (CAA) is considered an excellent surface pretreatment for Ti-6Al-4V adherends for adhesive bonding; however, some studies, as discussed in sections 2.4 and 2.5, suggests that the CAA oxide coating is unstable at high temperatures. Most of the work was carried out at high temperatures (>400°C) in vacuum or in air at about 300°C. However, there is insufficient information on the thermal stability of CAA oxide coatings on titanium in the temperature range, 350°C to 400°C. This temperature range is of interest for adhesive bonding because many high performance adhesives cure at a relatively high temperatures. For example, FM-5 adhesive used in the present study cures at 350°C. When a high temperature curing adhesive is used for adhesive bonding the thermal stability of the adherend surface coating becomes an important issue, even though the bonded joints may never be exposed to high

temperature in the service environment. The adherend surface coating must be thermally stable at the cure temperature for a time long enough for the adhesive to cure.

The presence of fluoride ions in the anodic oxide coatings is detrimental to the bond durability of adhesively bonded aluminum joints. The fluoride ion in the anodic oxide coating is believed to play a significant role in the durability of adhesively bonded titanium joints. However, the role of fluoride ions on the strength and durability of adhesively bonded titanium joints has not been investigated. First of all, the chemical nature of the fluoride ions in the oxide coatings of CAA treated Ti-6Al-4V alloy is not properly known. Fluoride ions in the oxide coatings of CAA treated titanium alloy could attack metals and their oxides to form fluorides and or oxyfluoride species. As discussed in section 2.6, the chemical reactions between hydrofluoric acid (HF) and the constituent elements, aluminum and titanium, of Ti-6Al-4V alloy and their oxides are at least thermodynamically favorable in the temperature range 298.15°K to 700°K. The formation of metal fluoride species in CAA oxide coatings and at metal/oxide interfaces could result in weakening of the oxide phase and/or the oxide/metal interface which could lead to bond failure under a minimal load. Unfortunately, research studies probing the role of fluoride ions on the strength and durability of CAA surface treated Ti-6Al-4V adherends exposed to high temperature environments have not been carried out.